THE UNIVERSITY OF CALGARY

MICROSTRIP DISCONTINUITY ANALYSIS

by

Wolfgang Oberhammer

A THESIS

SUBMITTED TO THE FACULTY OF GRADUATE STUDIES

IN PARTIAL FULFILLMENT OF THE REQUIREMENTS FOR THE

DEGREE OF MASTER OF SCIENCE

DEPARTMENT OF ELECTRICAL ENGINEERING

CALGARY, ALBERTA

MARCH, 1986

ISBN 0-315-30000-0

THE UNIVERSITY OF CALGARY

FACULTY OF GRADUATE STUDIES

The undersigned certify that they have read, and recommended to the Faculty of Graduate Studies for acceptance, a thesis entitled, "*Microstrip Discontinuity Analysis*" submitted by Wolfgang Oberhammer in partial fulfillment of the requirements for the degree of Master of Science.

Supervisor - Dr. R.H. Johnston
Dept. of Electrical Engineering

Ronald H Johnston

Dr. D. Irvine-Halliday
Dept. of Electrical Engineering

David Irvine-Halliday

Dr. K.V.I.S. Kaler
Dept. of Electrical Engineering

David L. Fry

Dr. D.J. Fry
Dept. of Physics

Date: March 3/86

Abstract

In this thesis an equivalent circuit suitable for calculating scattering parameters of microstrip discontinuities is developed. It is found that in addition to the modes accounted for in dispersion models (TEM and surface waves), in the vicinity of some microstrip discontinuities, slab waveguide modes are significant. It is shown that a two dimensional LC-transmission line equivalent circuit, whose elements are evaluated using a dispersion model, can account for all significant modes present in such discontinuities. Scattering parameters of a large variety of discontinuities analyzed with this equivalent circuit are in good agreement with those measured or calculated with more complex models.

Radiation conductances derived for microstrip open circuits are successfully transformed for use in microstrip corners. It is postulated that this transformation is equally valid for other discontinuities such as steps and T-junctions.

Acknowledgements

The author is indebted to Dr. R. H. Johnston for his guidance, assistance and patience throughout the course of this work. Many thanks are also extended for financial assistance provided by the University of Calgary in the form of research and teaching assistantships. The cooperation received from the Electrical Department as a whole is very much appreciated. In particular, appreciation is extended to Mr. Garry Harrington for his skill and cooperation in producing microstrip components, and Laura Millan for her help with the typesetting.

Without the cooperation of the author's wife and children, this work would not have been possible. This thesis is dedicated to them.

DEDICATION

Dedicated to my wife, WaiPing,
my children, Trevor and Jennifer
for their love and understanding.

Table of Contents

Table of Contents (continued)

List of Tables

List of Figures

LIST OF SYMBOLS

A	Scalar coefficient
$\vec{A}$	Magnetic vector potential
B	Scalar coefficient
C	Capacitance
C'	Capacitance per unit length
$\vec{D}$	Electric flux density
$\vec{E}$	Electric field vector
E_x, E_y, E_z	Cartesian components of electric field
F	Form factor
F_{oc}	Form factor for open circuit
F_c	Form factor for corner
G	Green's function
G_r	Radiation conductance
G_s	Surface wave conductance
$\vec{H}$	Magnetic field vector
H_x, H_y, H_z	Cartesian components of magnetic field
I	Current
I_{mo}, I_{po}	Expansion coefficients
$\vec{J}$	Current density

L	Inductance
L'	Inductance per unit length
P	Power (radiated)
P_{oc}	Power radiated from open circuit
R_{rad}	Radiation resistance
S_{ij}	Scattering parameter from port j to port i
S	Voltage standing wave ratio
T	Ratio of substrate surface wave to incident field power
U_{mo}, U_{po}	Expansion coefficients
V	Voltage
V	Volume (used to denote volume integrals)
V_{inc}	Voltage of incident signal
V_{oc}	Voltage at open circuit termination
V_m	Voltage at matched termination
V_{TEM}	Conductor voltage due to *TEM* mode
$V_{TE_{k0}}$	Conductor voltage due to TE_{k0} mode
W	Substrate width
Y	Admittance
Z_o	Characteristic impedance
c	Speed of light in free space
f	Frequency

k	Wave number as used by Lewin
h	Substrate height
n	Number of nodes per width in equivalent circuit
t	Substrate height as used by Lewin
w	Conductor width
w_{eff}	Effective conductor width
Φ	Electric scalar potential
Ψ_{k0}	Scalar potential for TE_{k0} modes
Γ	Reflection coefficient
η_o	Intrinsic impedance of free space
β	Wave number
ε_o	Permittivity
ε_r	Relative permittivity
ε_{eff}	Effective relative permittivity
γ	Propagation constant
ρ	Charge density
σ	Electric conductivity
μ_o	Permeability of non-magnetic materials
μ	Permeability
ω	Angular frequency
ω_c	Angular cut-off frequency of TE_{10} mode

CHAPTER 1

MICROSTRIP ANALYSIS

1.1. Introduction

With the development of solid state devices capable of operating at microwave frequencies and the ongoing miniaturization of electronic equipment, the microstrip transmission line has became a very attractive alternative to waveguides, coaxial lines and strip transmission lines.

The planar structure (see Fig. 1.1) of the microstrip transmission line makes it ideal for microwave integrated circuits. A microstrip line network is built in a single plane. The impedance of the transmission line is controlled by the line width and the electrical length of the line is controlled primarily by the physical length of the line. Complex microwave circuits can be constructed using microstrip lines as a medium. These circuits may be built using printed circuit board or thick film fabrication techniques. Printed circuit technology can, thus, be applied in microstrip circuit construction resulting in small size and low cost circuits.

While small size and low manufacturing cost has resulted in widespread application of microstrip transmission lines, theoretical analysis has proven to be very difficult. Transmission lines that do not have uniform dielectric filling cannot support a single mode of propagation. The abrupt air dielectric interface in

microstrip line gives rise to a complicated distribution of modes. The modal content of the propagating signal is also affected by the strip geometry. Because branches, steps, corners and other discontinuities are invariably present in microstrip circuits, it is of great importance to determine the effect of discontinuities on wave propagation.

Scattering parameters provide a very useful characterization of microstrip line discontinuities. A simple, yet effective method of determining the scattering parameters of microstrip discontinuities has already been developed [1]. This method which modelled the discontinuity as a rectangular section is, in this thesis, refined by the addition of transient sections at the input and output of the discontinuity. Further more, this method has been expanded to account for non-*TEM* (Transverse Electro-Magnetic) modes as well as radiation losses.

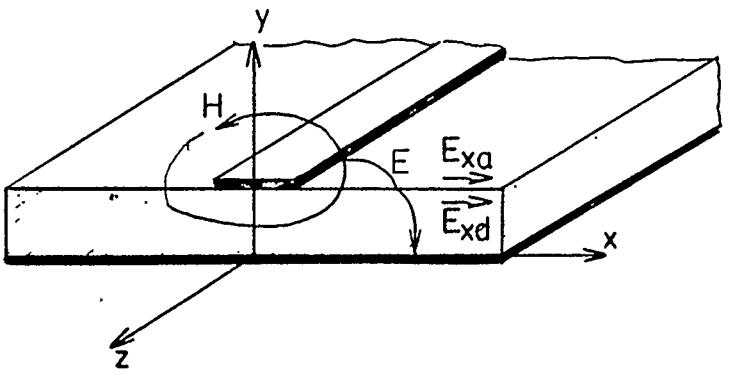

Figure 1.1 Microstrip Configuration

1.2. Wave Propagation in Microstrip Lines

It is of interest to illustrate the non-*TEM* behavior of the microstrip line as per Gupta et al [2]. Applying the continuity condition of a tangential component of electric field along the dielectric-air interface as shown in Fig. 1.1 gives:

$$E_x|_d = E_x|_a \tag{1.1}$$

$$\nabla \times \vec{H} = \frac{\partial \vec{D}}{\partial t} = \varepsilon_r \frac{\partial \vec{E}}{\partial t} \tag{1.2}$$

Where d and a stand for the dielectric and air respectively

$$\bar{a}_x \cdot \left\{ \nabla \times H \right\}_d = \bar{a}_x \cdot \left\{ \varepsilon_r \nabla \times H \right\}_a \tag{1.3}$$

$$\varepsilon_r \frac{\partial H_z}{\partial y}|_a - \frac{\partial H_z}{\partial y}|_d = \left\{ \varepsilon_r - 1 \right\} \frac{\partial H_y}{\partial z} \tag{1.4}$$

When $\varepsilon_r \neq 1$ equation (1.4) implies that the expression on the left side be a nonzero quantity, therefore $H_z \neq 0$.

The above analysis clearly illustrates that due to the fringing component of the E_x and H_x fields at the dielectric-air interface, pure *TEM* propagation is not possible.

Similarly it can be shown that $E_z \neq 0$. It follows that the *TEM* mode can only exist along with *TE* and *TM* substrate surface modes.

In most microstrip lines used in industry the spacing between the ground plane and conducting strip is much less than half a wavelength. Hence, the tangen-

tial component of the electric field must vanish in the vicinity of the conductor. This means that no *TM* waveguide mode can exist in these microstrip lines. Commonly, strip width is much larger than substrate height. Therefore, in addition to the *TE* and *TM* substrate surface modes, which in conjunction with the *TEM* mode form the dominant *TEM* hybrid mode, one or more *TE* waveguide modes may be present.

Numerous ways of modeling the various modes in microstrip lines have been developed. Only the methods relevant to this thesis are considered in the following section.

1.3. Background

High frequency circuits differ from conventional circuits largely because the short wavelength involved allows circuit components to be a substantial fraction of a wavelength in size. Stub tuners, filters, matching stubs and many other components can be incorporated geometrically. The typical microstrip circuit, thus, consists of a maze of conducting strips on a substrate with active components inserted and connected. Microstrip discontinuities, therefore, form a common and important part of every microstrip circuit. The scattering parameters (reflection and transmission coefficients) of discontinuities must be evaluated in the course of any microstrip circuit design.

At the dielectric-air interface the longitudinal components of the electric and magnetic fields are much smaller than their normal components. This observation

has led to the Quasistatic Analysis approach, which is based on the assumption that pure *TEM* mode propagation exists.

In distinction with the above method the Fullwave Analysis attempts to consider all modes present. This is done by decomposing the fields into *TE* and *TM* space harmonics, with each harmonic satisfying the wave equation and the boundary conditions with the conducting strip removed. The conducting strip is replaced by a strip of sheet current. The coupled pair of integral equations so formed are solved numerically.

A practical compromise between these two approaches is the widely used Planar Waveguide Model. This model originates from the Quasistatic approach. Parameters, however, are calculated with semiempirically derived expressions that account for dispersion. Dispersion is caused by the *TE* and *TM* modes. These modes become significant at higher frequencies, resulting in a wave number β that is a nonlinear function of ω. The Quasistatic Analysis and the Planar Waveguide Model and its application are detailed below.

1.3.1. Quasistatic Analysis

A discontinuity in a microstrip line consists of an abrupt change in geometry. The altered electric field distribution gives rise to a change in capacitance. The altered magnetic field distribution changes the current distribution in the strip and can be modeled with additional inductance. Hence a common way of modeling a discontinuity is by an equivalent circuit, consisting of capacitors and inductors that

account for the total change in the electric and magnetic fields.

A large number of methods for evaluating equivalent capacitance and inductance of discontinuities have been developed. Silvester and Benedik [3] calculated the potential Φ of a line using Green's function G and assuming a line charge configuration ρ along the microstrip line.

$$\Phi = \int_V \rho \, G \, dV$$
$$G = \frac{1}{4\pi|\vec{R} - \vec{R}_o|} \tag{1.5}$$

To avoid computational difficulties they compute the potential of two infinite lines. One of the lines has a uniform charge distribution the other has charge reversal at the origin. The sum of these potentials gives the equivalent of an open circuited line. This approach can be generalized to encompass various other discontinuities. The capacitance C of the line is evaluated from:

$$C = \frac{\int \rho dx}{\Phi} \tag{1.6}$$

Thompson and Gopinath [4] calculated the equivalent inductances of various microstrip discontinuities. Using the magnetic vector potential $\vec{A}$ and Maxwell's equations.

$$\vec{A} = \mu_o \int_V G \, \vec{J} \, dV \tag{1.7}$$

$$\vec{E} = -\frac{\partial \vec{A}}{\partial t} - \nabla\Phi \tag{1.8}$$

$$\vec{J} = \sigma \vec{E} \tag{1.9}$$

$$\vec{J} + \sigma \mu_o \frac{\partial}{\partial t}\left[\int_V G \vec{J}\, dV\right] = -\sigma \nabla\Phi \tag{1.10}$$

where σ is the conductance of the strip conductor.

For microstrip lines σ is very large and the frequency of operation is very high, therefore, current density $\vec{J}$ can be neglected and equation (1.10) becomes,

$$\mu_o \frac{\partial}{\partial t}\int_V G \vec{J}\, dV \approx -\nabla\Phi \tag{1.11}$$

Evaluating the electric potential using Laplace's equation they find Φ, $\vec{J}$ and $\vec{A}$. From

$$\int_V \vec{A} \cdot \vec{J} dV = I^2 L \tag{1.12}$$

the inductance is evaluated.

Gupta et al. [5] have given a closed form expression for capacitance and for inductance. According to these expressions, for a symmetric corner,

for $\frac{w}{h} > 1$

$$\frac{C}{w} = (9.5\varepsilon_r + 1.25)\frac{w}{h} + 5.2\varepsilon_r + 7.0 \quad \frac{pF}{m} \tag{1.13}$$

$$\frac{L}{h} = 100\left\{4\left\{\frac{w}{h}\right\}^{1/2} - 4.21\right\}\frac{nH}{m} \tag{1.14}$$

Equations (1.13) and (1.14) apply to the discontinuity shown below.

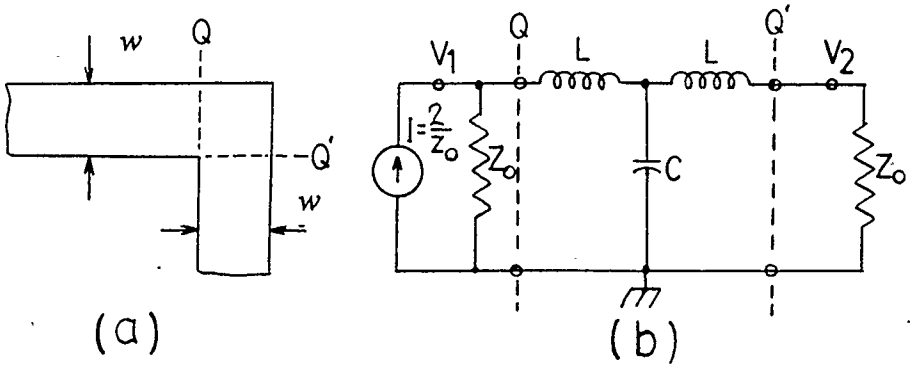

Figure 1.2 a) Microstrip Corner.
b) Equivalent Circuit of Corner.

The quasistatic analysis is accurate only for low frequencies. The equivalent circuit in Fig. 1.2 may be used for calculating the scattering parameters of the discontinuities it models. If Z_o is matched in each leg of Fig. 1.2, equations (1.13) and (1.14) give the scattering parameters as a function of frequency.

$$S_{11} = V_1 - 1.0 \tag{1.15}$$

$$S_{21} = V_2 \tag{1.16}$$

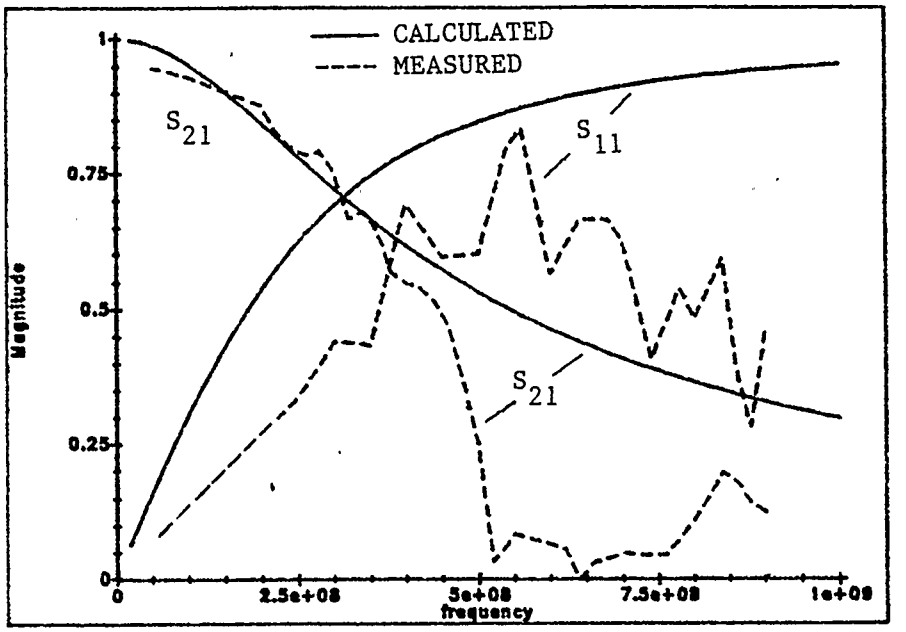

Figure 1.3 Scattering Parameters Calculated from Quasistatic Model

Comparing these results with measurements, we find quasistatic analysis gives a reasonable approximation of scattering parameters at low frequencies but fails to predict cutoff frequencies, null points or other important information.

1.3.2. Planar Waveguide Model

Wheeler has shown through conformal mapping techniques, that the open field region of the microstrip line can be transformed into the field region of a waveguide. This waveguide consists of two parallel strip conductors of effective width w_{eff} and magnetic walls of height h.

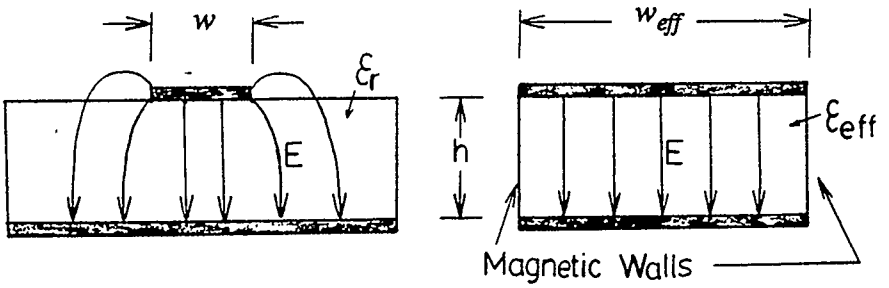

w = strip width

ε_r = dielectric constant

w_{eff} = effective strip width as derived by conformal mapping

ε_{eff} = effective dielectric constant

Figure 1.4 a) Cross Section of Microstrip Line.
b) Waveguide Model for Microstrip Line.

The planar waveguide model derivation is based essentially on the separate evaluation of inductance and capacitance along the line. This analysis is valid if substantially all of the energy transmitted is in the *TEM* mode. Wheeler's waveguide model is thus derived from quasi-static analysis. In order to account for dispersion, Wheeler's model is modified by incorporating frequency dependent effective widths and dielectric constants.

An expression for characteristic impedance is given by Hammerstad [6]:

$$Z_0 = \frac{\eta_0}{\sqrt{\varepsilon_{eff}}} \left[\frac{w}{h} + 1.393 + 0.667 \ln\left[\frac{w}{h} + 1.444\right]\right]^{-1} \tag{1.17}$$

and the effective dielectric constant is

$$\varepsilon_{eff}(0) = \tfrac{1}{2}\left[\varepsilon_r + 1 + \frac{\varepsilon_r - 1}{(1 + 12\,\frac{h}{w})^{1/2}}\right] \tag{1.18}$$

where $\eta_0 = 376.7$, $\varepsilon_r < 16$ and $\frac{w}{h} > 1.0$. The conductor thickness is assumed to be zero. $\varepsilon_{eff}(0)$ and $w_{eff}(0)$ apply at low frequencies where the frequency dependence is small.

The effective width of the line may be shown from the above expressions to be,

$$w_{eff}(0) = \frac{h\,\eta_o}{Z_o\,\varepsilon_{eff}(0)^{1/2}} \tag{1.19}$$

The two parameters (w_{eff} and ε_{eff}) are frequency dependent. Owens [7] gives the high frequency effective width as,

$$w_{eff}(f) = w + \frac{w_{eff}(0) - w}{1 + \left[\frac{f}{f_p}\right]^2}\ , \tag{1.20}$$

where

$$f_p = \frac{c}{2w_{eff}(0)\sqrt{\varepsilon_{eff}(0)}} \quad .$$

and

$$c = 3 \times 10^8 m/s$$

Schneider [8] presents an expression for the frequency dependence of the dielectric constant,

$$\varepsilon_{eff}(f) = \frac{\varepsilon_{eff}(0)\varepsilon_r(1 + \left[\frac{f}{f_c}\right]^2)^2}{(\varepsilon_r^{1/2} + \varepsilon_{eff}(0)^{1/2} f^2/f_c^2)^2} \tag{1.21}$$

where

$$f_c = \frac{c}{4h\sqrt{\varepsilon_r - 1}}$$

1.3.3. Full Wave Analysis

Wolf, Kompa and Mehran [9] used the planar waveguide model for microstrip lines to calculate the scattering parameters for various microstrip discontinuities. Their method of analysis is based on mode matching. The mathematical formulation for mode matching is quite intricate. Therefore, a simple example is used to outline this method.

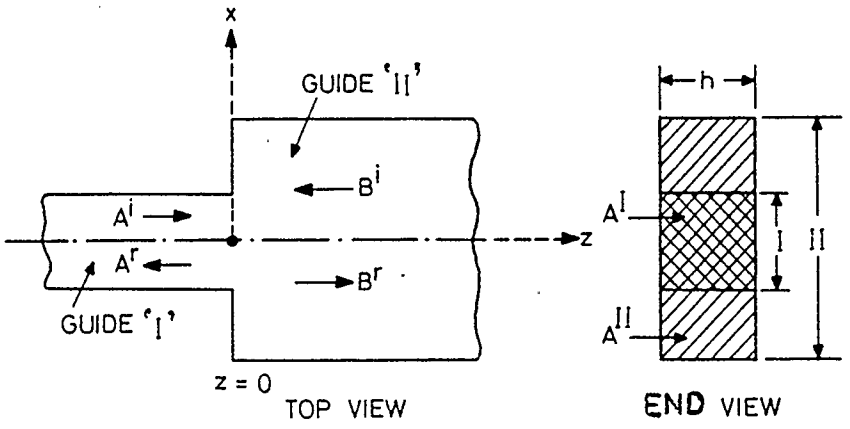

Figure 1.5 Microstrip Step

For the simplest case, a step, one surface constitutes the discontinuity. Electric and magnetic fields are given by:

$$E_t = \sum_{m=0}^{\infty} U_{m0} \left\{ \vec{z} \times \nabla_t \Psi_{m0}(x,y) \right\} \tag{1.22}$$

$$H_t = \sum_{m=0}^{\infty} I_{m0} \left\{ -\nabla_t \Psi_{m0}(x,y) \right\} \tag{1.23}$$

Equations (1.22) and (1.23) represent four field solutions - the incident and reflected electric and magnetic fields on either side of the discontinuity.

The boundary conditions at the common surface of the two lines are given by:

$$H_t^I = H_t^{II} \qquad in \ region \ A^I \tag{1.24}$$

$$E_t^I = E_t^{II} \quad in \ region \ A^I \tag{1.25}$$

$$H_t^{II} = 0 \quad in \ region \ (A^{II} - A^I) \tag{1.26}$$

Multiplying equation (1.25) by $\left\{ \vec{z} \times \nabla_t \Psi^I_{M0} \right\}$ and integrating over the aperture A^I, shown in Fig. 1.5, gives:

$$U^I_{M0} = \iint_A E_t^{II} \cdot \left\{ \vec{z} \times \nabla_t \Psi^I_{M0} \right\} dA \tag{1.27}$$

similarly:

$$I^{II}_{P0} = \iint_A H_t^I \cdot \left\{ - \nabla_t \Psi^{II}_{P0} \right\} dA \tag{1.28}$$

where M, m and P, p correspond to the modes of guides I and II respectively.

Due to orthogonality the summation reduces to a single term. Taking the dot product of a vector with itself reduces it to a scalar. Integration over the surface of the discontinuity the expansion coefficient can be isolated. Substituting E_t^{II} and H_t^I from equations (1.24) and (1.25) gives:

$$U^I_{M0} = \iint_A U^{II}_{p0} \cdot \left\{ (\vec{z} \times \nabla_t \Psi^{II}_{p0}) \cdot (\vec{z} \times \nabla_t \Psi^I_{M0}) \right\} dA \tag{1.29}$$

$$I^{II}_{P0} = \iint_A H_t^I \cdot \left\{ (- \nabla_t \Psi^I_{m0}) \cdot (- \nabla_t \Psi^{II}_{P0}) \right\} dA \tag{1.30}$$

At this point the expansion coefficients can be expressed in terms of the mode coefficients.

$$\sqrt{Z^{I}_{M0}}\,(A^{i}_{M0}+A^{r}_{M0}) = \sum_{p=0}^{\infty}\sqrt{Z^{II}_{p0}}\left\{\iint_{A}(\vec{z}\times\nabla_t\,\Psi^{II}_{p0})\cdot(\vec{z}\times\nabla_t\,\Psi^{I}_{M0})\,dA\right\}(B^{i}_{p0}+B^{r}_{p0}) \tag{1.31}$$

$$\sqrt{Y^{II}_{P0}}\,(B^{i}_{P0}-B^{r}_{P0}) = \sum_{m=0}^{\infty}\sqrt{Y^{I}_{m0}}\left\{\iint_{A}(\nabla_t\,\Psi^{I}_{m0})\cdot(\nabla_t\,\Psi^{II}_{P0})dA\right\}(A^{i}_{mo}-A^{r}_{mo}) \tag{1.32}$$

where ∇_t is the transverse component of the gradient.

By truncating equation (1.32) and solving for the *TEM* mode coefficients one can determine the scattering parameters using,

$$\begin{bmatrix}A^{r}\\B^{r}\end{bmatrix} = \begin{bmatrix} & S & \end{bmatrix}\begin{bmatrix}A^{i}\\B^{i}\end{bmatrix} \tag{1.33}$$

where A and B are the coefficients of the incident and reflected electric and magnetic fields as defined in Fig. 1.5.

Results of the above analysis are shown in Chapter 2 section 4. While the results give excellent agreement with experimental data, the analysis is formidably complex even for the simplest of geometries. A good compromise between the complexity of the analysis and the accuracy of the results is found using 2-

dimensional transmission line equivalent circuits as detailed in the remaining chapters.

CHAPTER 2

EQUIVALENT CIRCUIT FOR MICROSTRIP DISCONTINUITIES

2.1. Simplified Mode Distribution

The object of this chapter is to develop a simple, yet accurate method of predicting scattering parameters of microstrip discontinuities. The quasi-static models, deal only with *TEM* or quasi-*TEM* mode and are, therefore, inadequate for calculating the high frequency scattering parameters of discontinuities. Fullwave Analysis, on the other hand, gives excellent results but its application is too complex for many engineering applications. Limiting the application of the model to microstrip lines commonly used in industry, the number and types of modes considered in the analysis can be reduced. Taking only the modes that contain a significant portion of the signal energy into consideration, the analysis can be simplified with a small loss in accuracy.

Today, microstrip transmission lines are used for frequencies up to 30 GHz and higher. For a 20 Ω line on a 1.56 mm substrate with dielectric constant of 2.32, the cut-off frequency of the TE_{10} mode is about 6.2GHz. For 50 Ω line on the same substrate this cut-off frequency is about 18 GHz. Measurements show that at these frequencies the scattering parameters change very abruptly, indicating that energy is coupled into an appropriate *TE* mode. For most microstrip lines the cut-off frequency of the lowest order TM-mode is outside the frequency range of

interest. It follows, that for frequencies above the lowest *TE* cut-off frequency propagation can be thought of as a superposition of the hybrid *TEM–TE–TM* mode plus one or more independent *TE* modes. That is, above the *TE* cut-off frequency, the microstrip line is both an inhomogeneous transmission line and a slab waveguide.

These observations led to the following simplifying assumptions:

- Only *TEM* and *TE* modes exist. To account for the fact that no pure *TEM* mode can exist, microstrip parameters are calculated using the planar waveguide dispersion model.
- *TE* modes exist only in the substrate; *TE* modes referred to in this chapter exist between conductor and ground plane and should not be confused with *TE* substrate surface modes.
- The substrate thickness is small compared to one wavelength.
- Conductor has infinite conductivity and zero thickness.
- Electric and magnetic fields are of the form

$$\vec{E} = \vec{E}_o\,(x,y)\; e^{j\omega t + \gamma z}$$

$$\vec{H} = \vec{H}_o\,(x,y)\; e^{j\omega t + \gamma z} \quad .$$

With the aid of these assumptions a simple circuit model is developed in the next two sections.

2.2. The Two Dimensional Transmission Line

The first clue of how to develop a model for microstrip discontinuities may come from an intuitive analysis of a simple discontinuity. The unperturbed wave propagating in a microstrip line is of a form that resembles a *TEM* mode. Consider now what happens when such a wave is incident upon a discontinuity such as the corner of Fig. 2.1

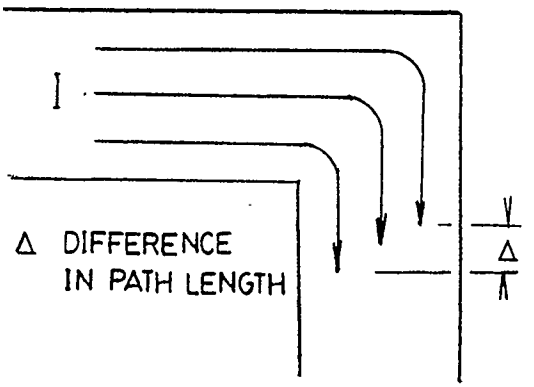

Figure 2.1 Approximate current flow in a microstrip corner.

At low frequencies essentially all the energy is transmitted across the discontinuity. Current in the strip can be thought of as traveling along a large number of discrete paths, all aligned in the same plane. The path length increases with distance from the inside edge of the conductor. This difference in path length introduces phase shifts between currents (or voltages) along adjacent path's. These

phase shifts are representative of the *TE* slab waveguide modes. Below the *TE* cut-off frequency, however, this phase shift cannot be sustained in the line emerging from the discontinuity. The discontinuity must, therefore give rise to a reflected wave that cancels the effect of phase shifts between adjacent current elements. This reflected wave is negligible at low frequencies where the phase shifts are small. As the frequency increases phase shifts and therefore reflections increase until the TE_{10} cut-off frequency is reached. Beyond the TE_{10} cut-off, most of the signal is transmitted across the discontinuity. The signal enters the discontinuity in form of a hybrid-*TEM* mode and emerges from the discontinuity in form of one or more *TE* modes.

The equivalent circuit in Fig. 2.2 is an expansion of the conventional *TEM* L-C ladder into a two dimensional circuit. Interconnecting two or more 2D-transmission lines at right angles, or whatever other configuration the discontinuity may assume, models current flow in the actual discontinuity. Parallel lines allow for phase shifts that arise with a change in current direction. Further, in the following analysis it will be shown, that this equivalent circuit can account for both, *TEM* and *TE* modes. This circuit will, thus, form the fundamental building block of the general circuit model to be developed in section 3 of this chapter.

2.2.1. TEM and TE Modes In Microstrip Lines

It is instructive to examine the two dimensional transmission line in Fig. 2.2. First the circuit will be analyzed while it is carrying the wave in the *TEM* mode,

and then it will be analyzed for transmission of higher order TE_{m0} modes. When only a *TEM* mode is present $\vec{J} = J_z$ since $H_z = 0$ hence no current flows in the shunt inductors of this equivalent circuit. The 2-D transmission line model, therefore, reduces to two parallel lines, where each is of the form of an equivalent circuit of a transmission line supporting pure *TEM* mode propagation.

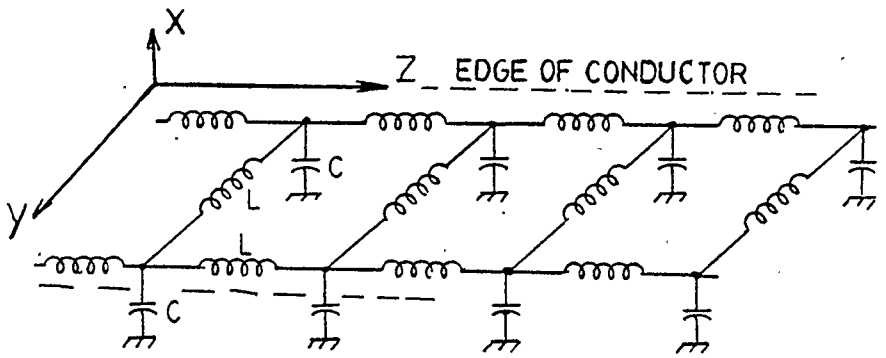

Figure 2.2 Two dimensional transmission line equivalent circuit.

Now let us assume only *TE* modes are present and all modes propagate in the z-direction. *TE* modes are contained in the substrate between conductor and ground plate, hence $E_y = E_z = 0$ when substrate thickness h is much less than $\frac{\lambda}{2}$. Applying Maxwell's equations we get:

$$\nabla \times \vec{E} = -j\omega\mu\vec{H} \tag{2.1}$$

$$\frac{\partial E_z}{\partial y} - \frac{\partial E_y}{\partial z} = 0 = -j\omega\mu H_x \tag{2.2}$$

hence $H_x = 0$

$$\gamma E_x = -j\omega\mu H_y \tag{2.3}$$

and

$$\frac{\partial E_x}{\partial y} = j\omega\mu H_z \tag{2.4}$$

The electric field only depends on x therefore the Helmholtz equation reduces to:

$$\frac{\partial^2 E_x}{\partial x^2} + (\gamma^2 - \omega^2\mu\varepsilon)\, E_x = 0 \tag{2.5}$$

a general solution to equation (2.5) is of the form:

$$E_x = A\ cos(ax) + B\ sin(bx) \tag{2.6}$$

$$\nabla \times \vec{H} = j\omega\varepsilon E_x \tag{2.7}$$

since $H_x = E_y = E_z = 0$

$$\frac{\partial H_z}{\partial x} = \frac{\partial H_y}{\partial x} = 0 \tag{2.8}$$

hence the magnetic field is independent of x and

$$H_z = J_y \tag{2.9}$$

At the edges of the conductor J_y must go to zero, and therefore H_z and $\frac{\partial E_x}{\partial y}$ must

be zero there. Equation (2.6) reduces to:

$$E_x = A\cos(\frac{\pi n}{w_{eff}}x) \tag{2.10}$$

where n = 1,2,3,···

Odd *TE* modes result in an asymmetric field distribution. Thus, if only odd *TE* modes are present the center of the conductor is at zero potential. Therefore the two dimensional transmission line equivalent circuit in Fig. 2.2 reduces to two parallel lines of the type shown in figure 2.3.

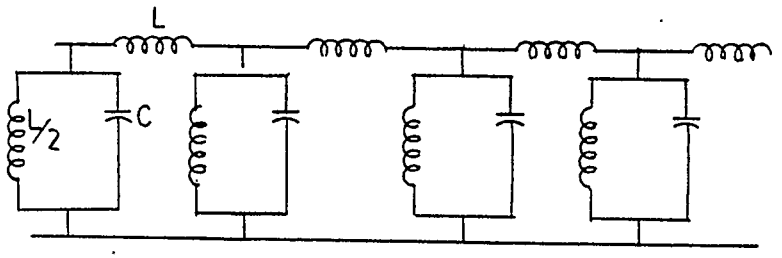

Figure 2.3 The equivalent circuit for *TE* modes.

The shunt admittance is given by

$$Y = j\omega C + \frac{2}{j\omega L} \tag{2.11}$$

$$Y = j\omega C(1 - \frac{2}{\omega^2 LC}) \tag{2.12}$$

note that L and C are $L' \times w_{eff}$ and $C' \times \frac{w_{eff}}{4}$ respectively. The primes denote per unit length quantities.

$$Y = j\omega C(1 - \left\{\frac{\omega^2{}_c}{\omega^2}\right\}) \tag{2.13}$$

where $\omega_c = \frac{\sqrt{2}}{\sqrt{LC}} = \frac{2\sqrt{2}}{w_{eff}\sqrt{L'C'}}$

The line in Fig. 2.3 is the equivalent circuit of a line supporting a pure *TE* mode with

$$\omega_c = \frac{2\sqrt{2}}{w_{eff}\sqrt{L'C'}}$$

while from conventional waveguide theory it can be shown that:

$$\omega_c = \frac{\pi}{w_{eff}\sqrt{L'C'}}$$

Greater accuracy can be achieved by using more nodes per width. For comparison, cut-off frequencies for circuits with 2 to 5 nodes per width are given in Table 2.1

Table 2.1. Comparison of Cut-off frequencies

Number of nodes per width in equivalent circuit	ω_c
infinite	$\frac{\pi}{w_{eff}\sqrt{L'C'}}$
2	$\frac{2\sqrt{2}}{w_{eff}\sqrt{L'C'}}$
3	$\frac{3}{w_{eff}\sqrt{L'C'}}$
4	$\frac{3.06}{w_{eff}\sqrt{L'C'}}$
5	$\frac{3.09}{w_{eff}\sqrt{L'C'}}$

It has been shown that the two dimensional transmission line model represents a line supporting both, *TEM* and *TE* modes. According to the assumptions made earlier in this chapter, with a 2D-equivalent circuit all modes likely to exist in a microstrip line can be modeled. This is of considerable significance since now boundary conditions and modal distribution can be determined by the circuit model.

2.3. Modeling Micro Strip Discontinuities

Sections of 2D-transmission line can be interconnected to form the same basic configuration of the microstrip discontinuity under consideration. Details of how to construct an equivalent circuit are given in the following subsections.

2.3.1. Mode Distribution in Discontinuities

In a microstrip discontinuity the number and type of modes generated are such that all boundary conditions are satisfied. As explained in section 2.1, only a *TEM*-hybrid and, depending on line width and wavelength, one or more *TE* modes may propagate in lines emerging from discontinuities. All nonpropagating modes are attenuated to low values within a short but finite section of each line leaving the discontinuity. That is, evanescent modes propagate a finite distance into lines emerging from a discontinuity before they vanish.

Scattering parameters for the *TEM* - hybrid mode change depending on what modes are propagating and what modes are reflected or attenuated. As far as scattering parameters are concerned, a discontinuity consists not only of the common area of two or more intersecting lines, but also it consists of the parts of each emerging line where evanescent modes can exist. The equivalent circuit of a discontinuity must reflect this consideration.

An equivalent circuit of a discontinuity can be formed by interconnecting $m + 1$ sections of 2D-transmission lines, where m is the number of conductors emerging from the discontinuity.

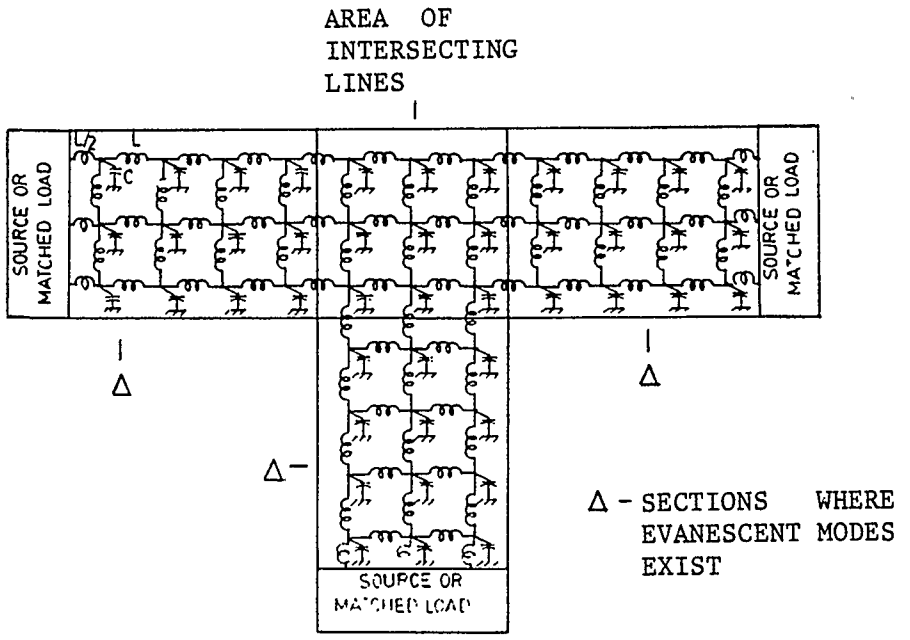

Figure 2.4 Sectioning the equivalent circuit.

In the interconnecting section, which accounts for the evanescent decaying higher order modes, phase shifts arise. These phase shifts between adjacent nodes are of interest. The *m* sections, representing the transient part of the *m* emerging lines, determine what modes can propagate in each line. That is, each section acts like an all-pass filter to the *TEM*, or in-phase component, and a high-pass filter to the *TE* component having an asymmetric phase distribution in parallel nodes.

As illustrated above, by sectioning the equivalent circuit, circuit operation can be understood more easily. Beyond that, the significance of sectioning lies in the separate evaluation of circuit parameters for each section. The separate evaluation

of circuit parameters allows for impedance changes between individual lines emerging from the discontinuity.

2.3.2. Evaluation of Circuit Parameters

Neglecting the possible presence of *TE* modes for a moment, the *TEM* equivalent circuit will be derived. The dominant mode is not a pure *TEM* mode and this is accounted for by using the planar waveguide model parameters to calculate circuit elements. The intrinsic impedance is given by:

$$Z_o = \left\{ \frac{L'}{C'} \right\}^{1/2} \tag{2.14}$$

The wave number is,

$$\beta = \omega\sqrt{L'C'} \tag{2.15}$$

$$= \frac{\omega\sqrt{\varepsilon_{eff}}}{c} \tag{2.16}$$

where c is the speed of light in free space.

Multiplying equation (2.14) by (2.15) and using equation (1.19) the inductance L' and capacitance C' can be determined.

$$L' = \mu_o\, h \tag{2.17}$$

$$C' = \frac{\varepsilon_o\, \varepsilon_{eff}\, w_{eff}}{h} \tag{2.18}$$

As shown in the last section, *TE*-modes can be accounted for by using a 2D-transmission line model. For the purpose of developing a 2D-model, the microstrip conductor surface is conceptually divided into square sections as shown in Fig. 2.5.

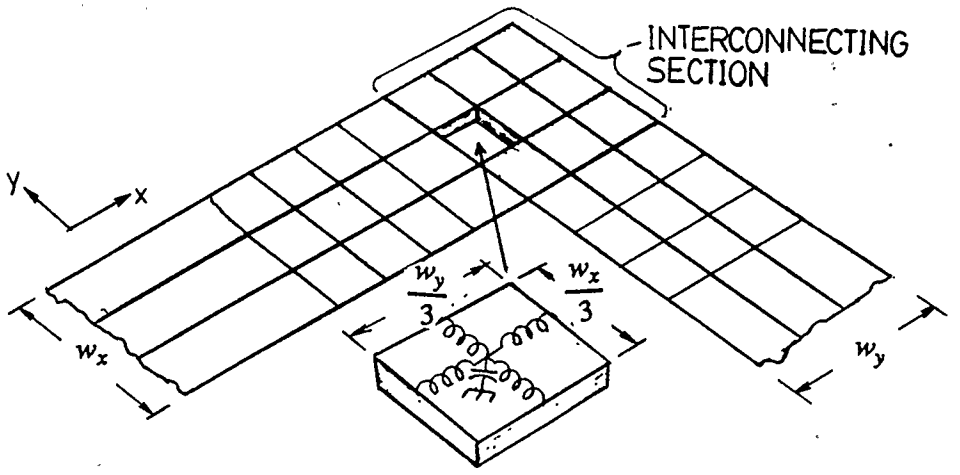

Figure 2.5 Segmentation of Microstrip Conductor.

The inductances L and the Capacitances C for the element in Fig. 2.5 are given by:

$$L = \frac{L' w_{eff}}{2} = \frac{h \eta_o}{c} \tag{2.19}$$

$$C = \frac{C' w_{eff}}{n^2}$$
$$= \frac{\varepsilon_o w_{eff}^2 \varepsilon_{eff}}{\eta_o h c n^2} \tag{2.20}$$

Where n is the number of elements per width. For discontinuities where lines of different impedances are connected perpendicular to one another, the elements of the interconnecting section are rectangular. Circuit parameters for this section are then calculated using equations (2.21) and (2.22)

$$L_x = \frac{\eta_o h w_{eff_y} n_x}{c w_{eff_x} n_y} \tag{2.21}$$

$$C = \frac{\varepsilon_o w_{eff_x} w_{eff_y} \sqrt{\varepsilon_{eff_x}} \sqrt{\varepsilon_{eff_y}}}{\eta_o h c n_x n_y} \tag{2.22}$$

Here all parameters that are a function of line width are calculated separately for each line. Subscripts x and y, therefore, indicate that the particular parameter is calculated for the line parallel to the x or y direction respectively.

2.3.3. Equivalent Circuit Construction

The last piece of information necessary for the development of an equivalent circuit, the selection of the number of nodes, is detailed in this section. The required number of nodes per width of a particular section depends on the waveguide modes expected to be present and the relative impedance between adjacent sections.

In the following chapter it will be shown that an n node per width equivalent circuit can account for the first $n-1$ TE modes. Depending on line width and maximum frequency of operation of the circuit a decision can be made as to what modes can exist in any line of the discontinuity under consideration. For a 50 Ω line on a substrate with $\varepsilon_r = 2.32$ that operates at less than 18GHz only the TE_{10} mode needs to be considered. Hence, for this line a two node per width equivalent circuit would suffice. In a 25 Ω line with the same substrate and frequency of operation, at least the two lowest order TE modes need to be considered. For this line the equivalent circuit must have at least 3 nodes per width.

The second criterion is based on the relative impedance between two lines that form a step discontinuity. To keep the circuit parameters of connected sections as similar as possible, the number of nodes should vary inversely with impedance from section to section. For example, a 50-25 Ω step discontinuity can be modeled with two sections. The section representing the 25 Ω line must have twice as many nodes per width as the 50 Ω section. Say, if two nodes per width are used in the 50 Ω section, four nodes per width are required in the 25 Ω section. To conform with the first criterion listed, this model is valid only if only the TE_{10} mode can exist in the 50 Ω line. In the 25 Ω line the TE_{10}, TE_{20} and the TE_{30} modes can be modeled, hence the number of nodes in the 50 Ω section is likely to be the limiting factor. This inverse relationship between number of nodes and impedance is not necessary for sections representing lines that are connected 90^o to one another. For example, each section of a 50-25 Ω corner can have the

same number of nodes per width although best accuracy is achieved if number of nodes for each line is related by a factor of two.

The last criterion for selecting the number of nodes has to do with computer time. Depending on facilities available and algorithms used in the circuit analysis computer time may or may not be a significant limitation. For the circuits given in the following section about 1 minute of VAX 750 CPU time was used per frequency point. It should, however, be mentioned that no effort was made to optimize the algorithm used. Even if computer time is not a significant limitation, data files for a large equivalent circuit are cumbersome to construct. In general, a lower number of nodes result in a faster and simpler analysis.

For reasons outlined in section 2.2 a minimum of 3 nodes per width is desirable. Where impedance changes are large between sections aligned in the direction of propagation, two nodes per width for the line with the higher impedance may be necessary to keep the number of nodes in the low impedance line at a reasonable limit. The number of nodes of the interconnecting section is determined by the larger of two possible adjoining sections in a given direction. Since interconnecting sections exist only in discontinuities where lines are connected perpendicular to one another, the number of nodes in the interconnecting section is determined by adjoining sections in both directions. The number of nodes per length of every section, except the interconnecting section, is strictly a trade-off between accuracy and computer time. Four nodes per length were used in every example given in this chapter.

Tee Equivalent Circuit

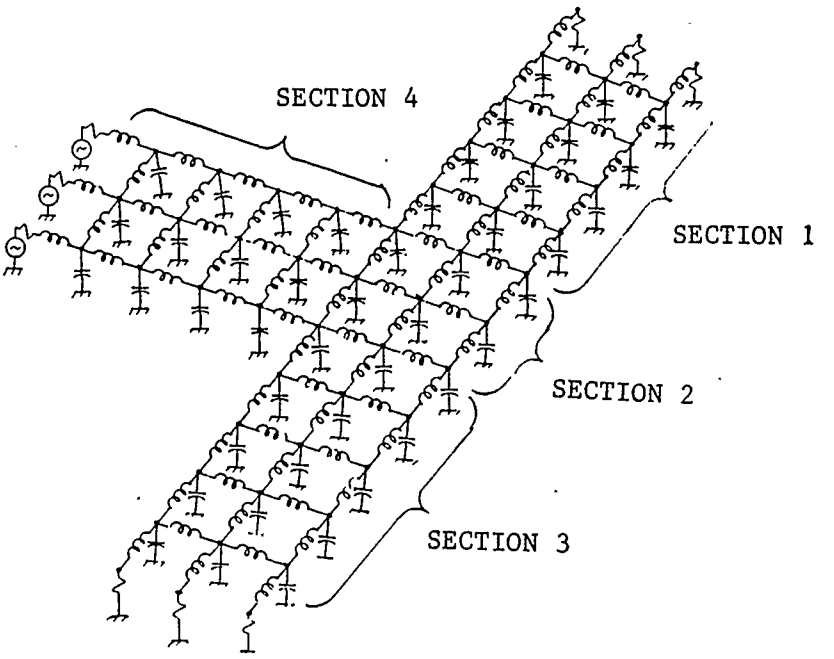

Figure 2.6 Equivalent Circuit Example.

The process of forming an equivalent circuit is now illustrated in an example. Fig. 2.6 shows the equivalent circuit of a symmetric Tee. The term symmetric implies that the intrinsic impedance of line 1 is the same as that of line 3. The line numbers correspond to the section numbers in Fig. 2.6. Assuming that, after deciding on the frequency range of operation and calculating cut-off frequencies of various modes, it has been established that only TE_{10} and TE_{20} modes can exist in any part of this discontinuity.

- Three nodes per width will account for all modes present;
- Impedance changes occur between lines connected perpendicular to one another, hence the number of nodes per width does not depend on relative impedance between lines.
- Three nodes per width and four nodes per length are chosen for sections 1, 3 and 4. The number of nodes of section 2 is determined by section 1 or 3 and section 4.

Further illustrations of the formation of equivalent circuits, are shown for various discontinuities considered in the next section.

2.4. Results

Scattering parameters of various discontinuities were computed. Conventional circuit analysis is used to determine the average voltage at each port of a discontinuity. The transmission coefficient is given by the average voltage at a output port. The reflection coefficient is given by $S_{11} = \vec{V}_{in} - 1$, where $\vec{V}_{in}$ is the average voltage of all nodes of the input port. The results are compared with those measured in the lab or published by other researchers [9],[10],[11]. All theoretical results used from the above references were calculated by the method of Fullwave Analysis. Both, the equivalent circuit used for the computation and the magnitude of the scattering parameters are given below for all discontinuities considered. None of the calculated results given in this Chapter include losses.

90° CORNER

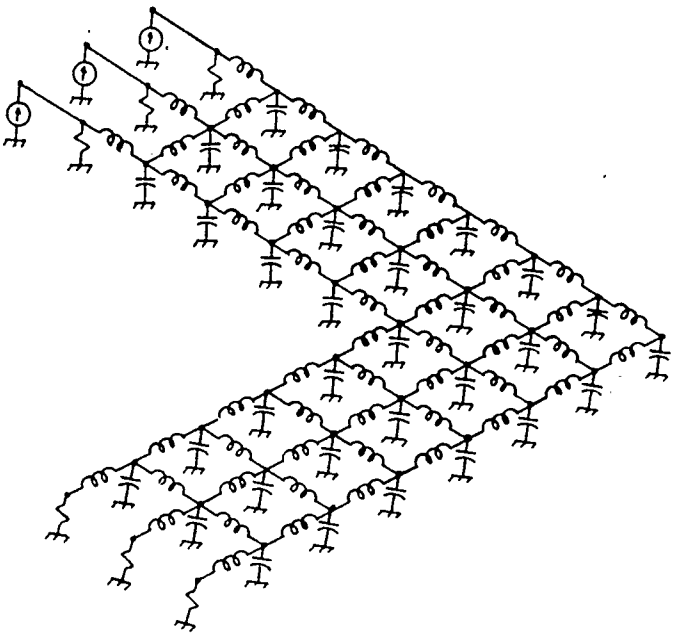

Figure 2.7 Equivalent Circuit for a 90° Corner

Any impedance change can be accommodated between perpendicular lines. Hence, a change in impedance does not affect the number of elements or nodes per width in each line. Fig. 2.7 shows the equivalent circuit used to calculate the magnitude and phase of the scattering parameters of a corner. The results are shown in Figs. 2.8 through 2.12.

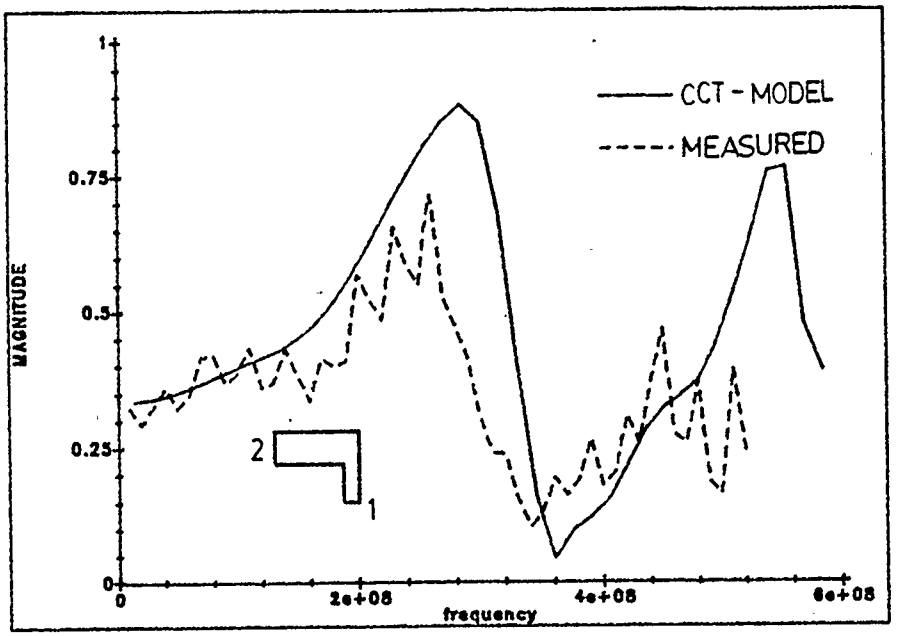

Figure 2.8 S_{11} for 50-25 Ω Corner $\varepsilon_r = 2.32$, $h = 3.81cm$

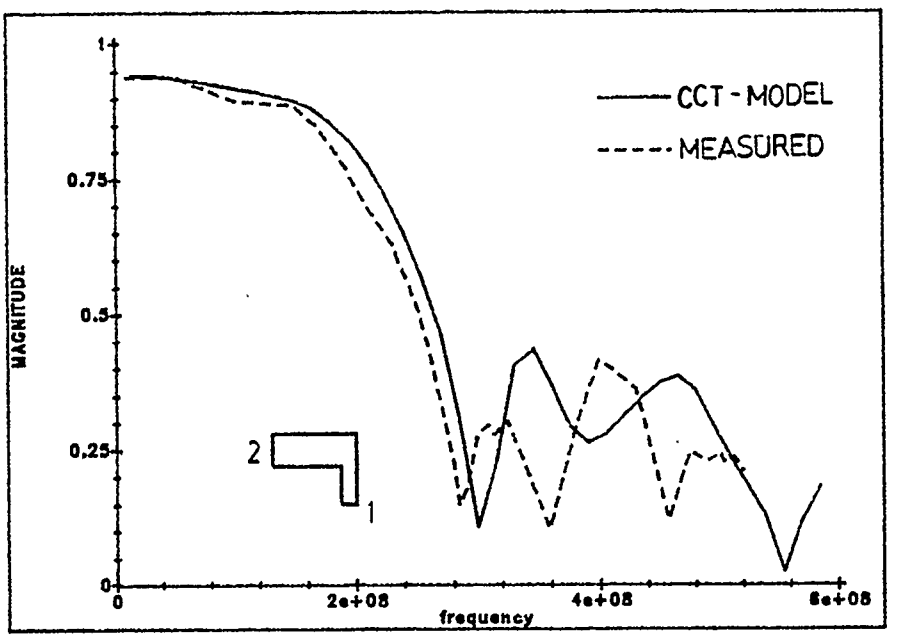

Figure 2.9 S_{21} for 50-25 Ω Corner $\varepsilon_r = 2.32$, $h = 3.81cm$

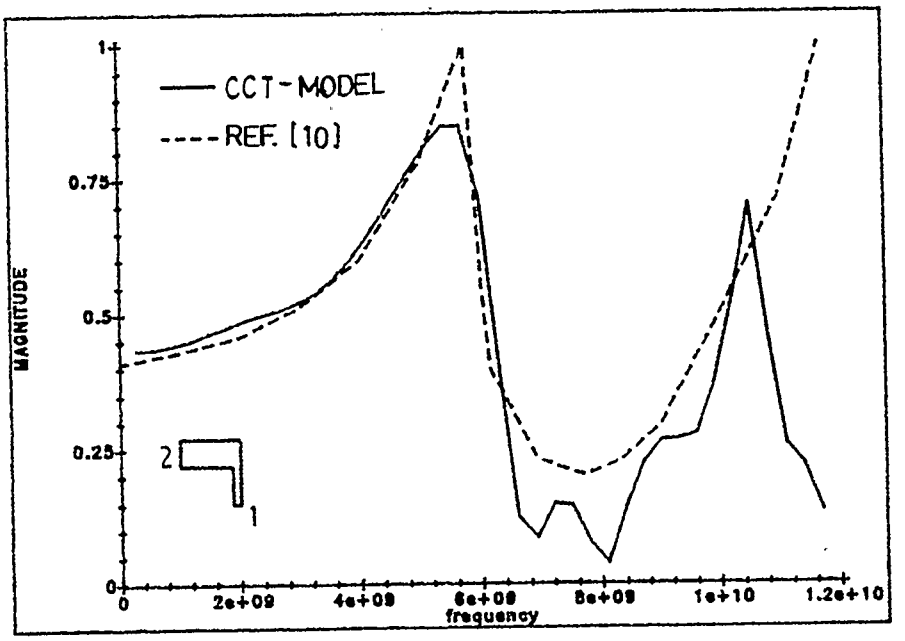

Figure 2.10 S_{11} for 50-20 Ω Corner $\varepsilon_r = 2.32$, $h = 0.156cm$

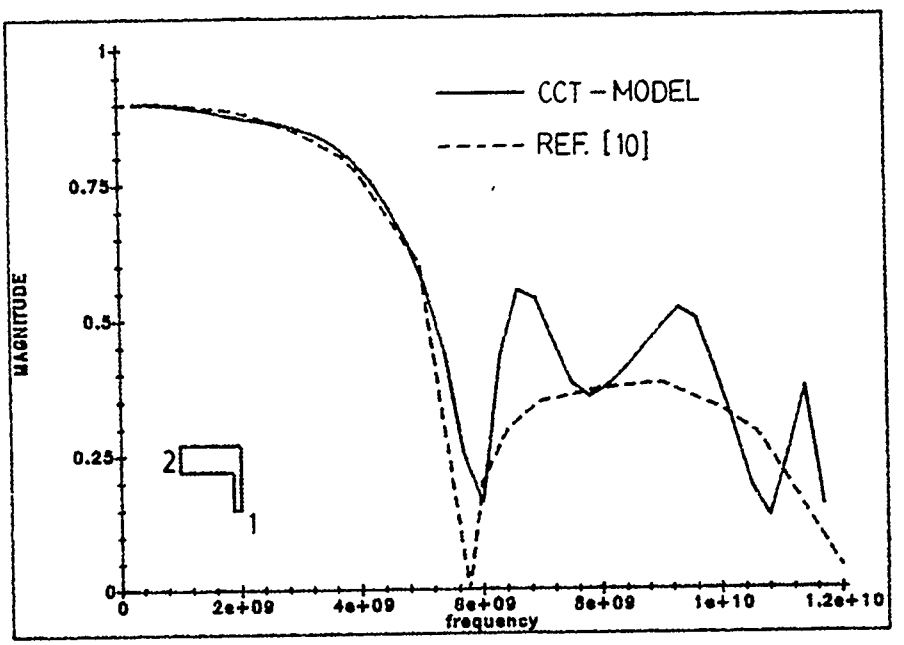

Figure 2.11 S_{21} for 50-20 Ω Corner $\varepsilon_r = 2.32$, $h = 0.156cm$

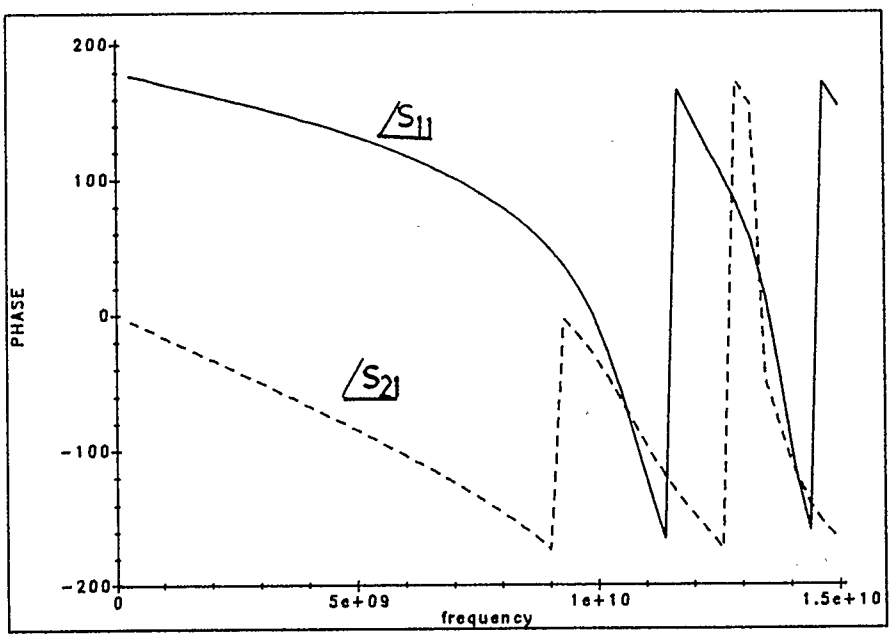

Figure 2.12 Phase of S_{11} and S_{21} 50-20 Ω Corner $\varepsilon_r = 2.32$, $h = 0.156cm$

Symmetric Tee

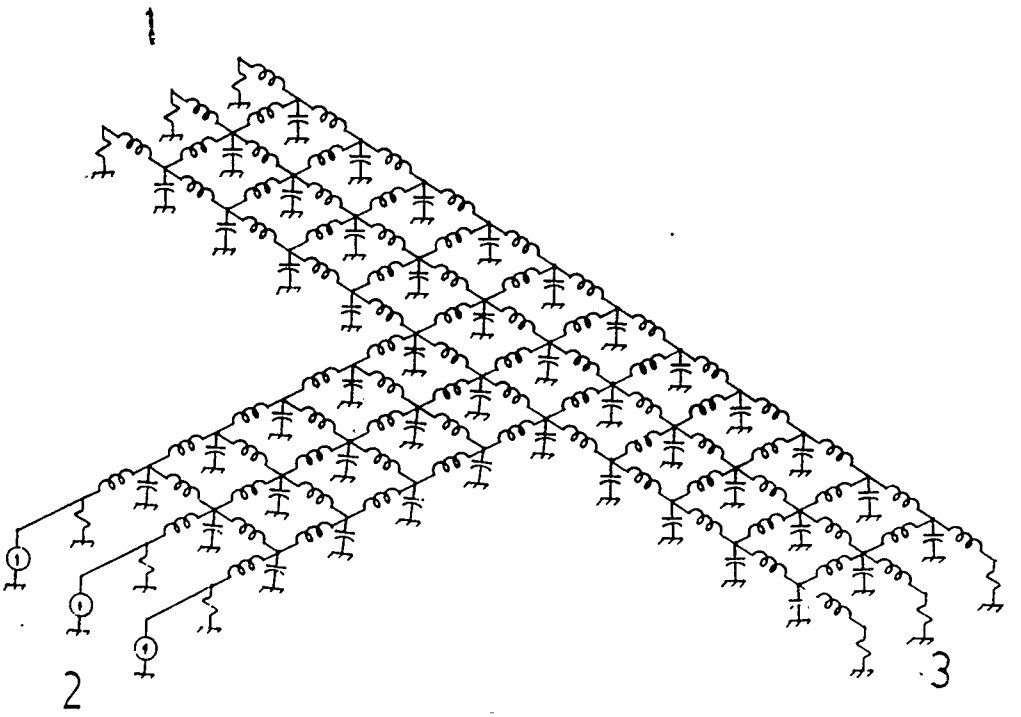

Figure 2.13 Equivalent Circuit for a 20-50-20 and 25-50-25 Ω Tee

Fig. 2.13 shows the circuit used for a 25-50-25 and a 20-50-20 Ω Tee. In both cases the signal enters from port 2, the 50 Ω terminal. Magnitudes and phase of scattering parameters are shown in Figs. 2.14 to 2.18.

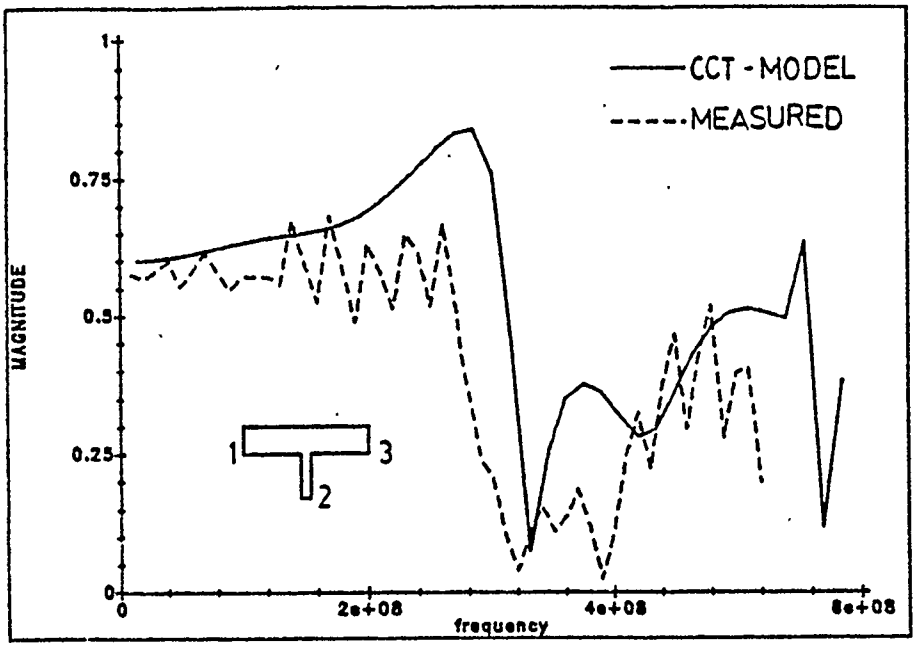

Figure 2.14 S_{22} for a 25-50-25 Ω Tee $\varepsilon_r = 2.32$ $h = 3.81cm$

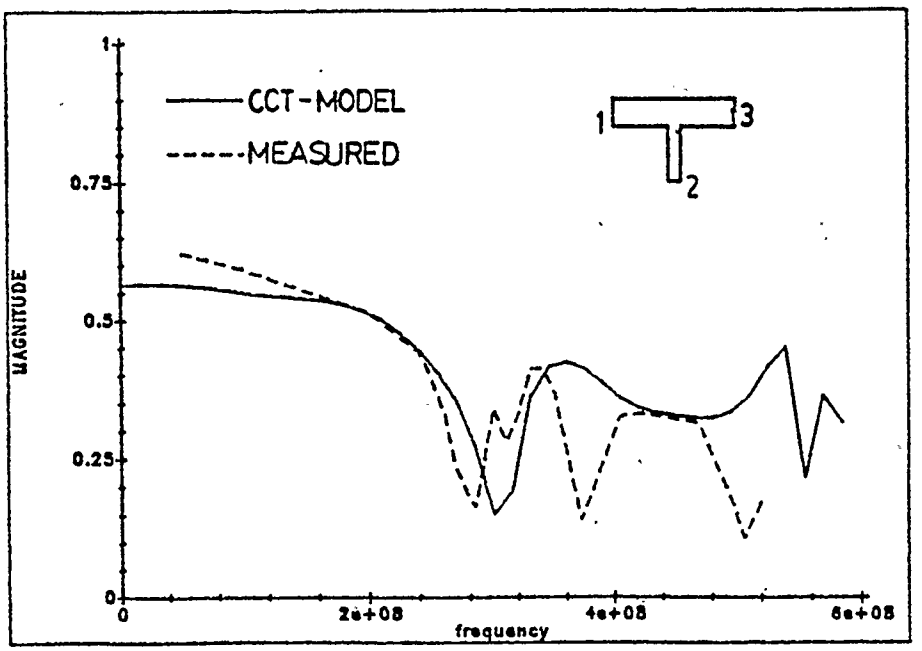

Figure 2.15 S_{12} for a 25-50-25 Ω Tee $\varepsilon_r = 2.32$ $h = 3.81cm$

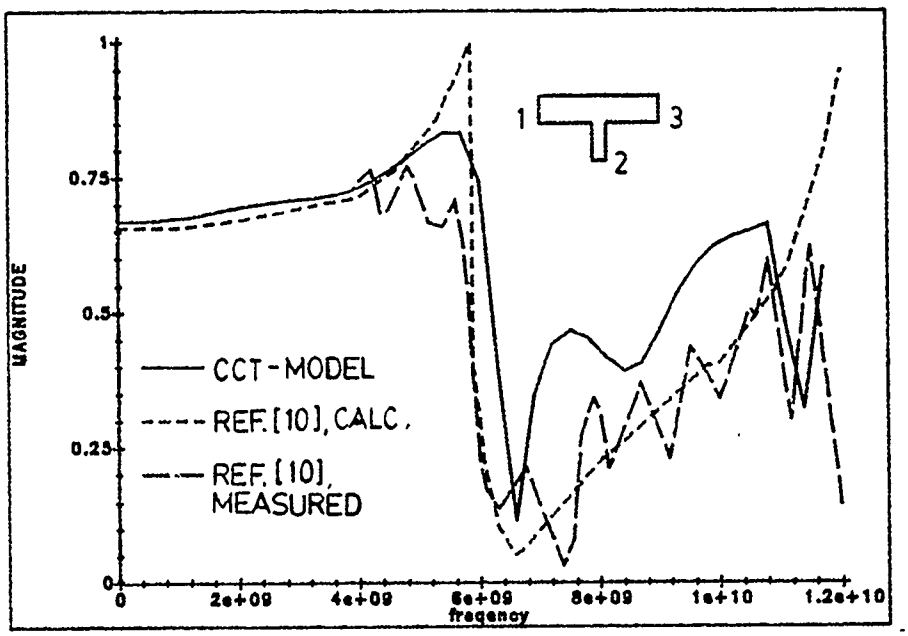

Figure 2.16 S_{22} for a 20-50-20 Ω Tee $\varepsilon_r = 2.32$ $h = 0.156cm$

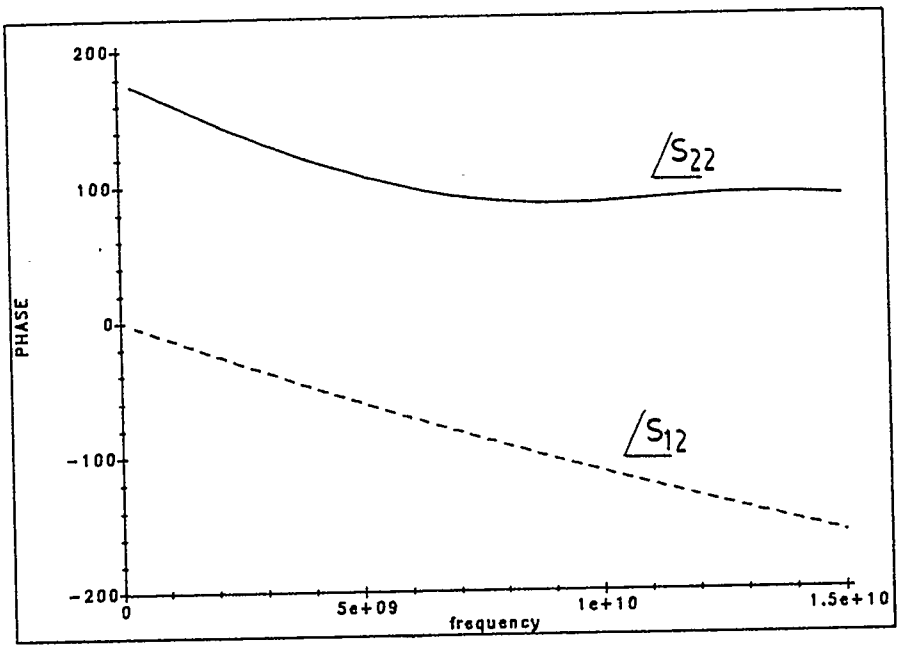

Figure 2.17 Phase of S_{22} and S_{12} for a 20-50-20 Ω Tee $\varepsilon_r = 2.32$ $h = 0.156cm$

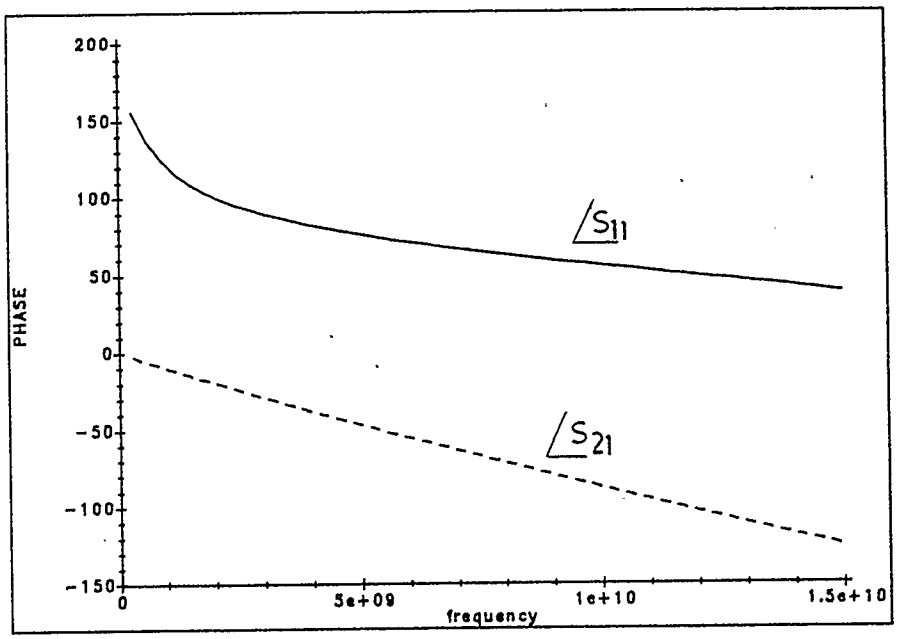

Figure 2.18 Phase of S_{11} and S_{21} for a 20-50-20 Ω Tee $\varepsilon_r = 2.32$ $h = 0.156cm$

Asymmetric Tee

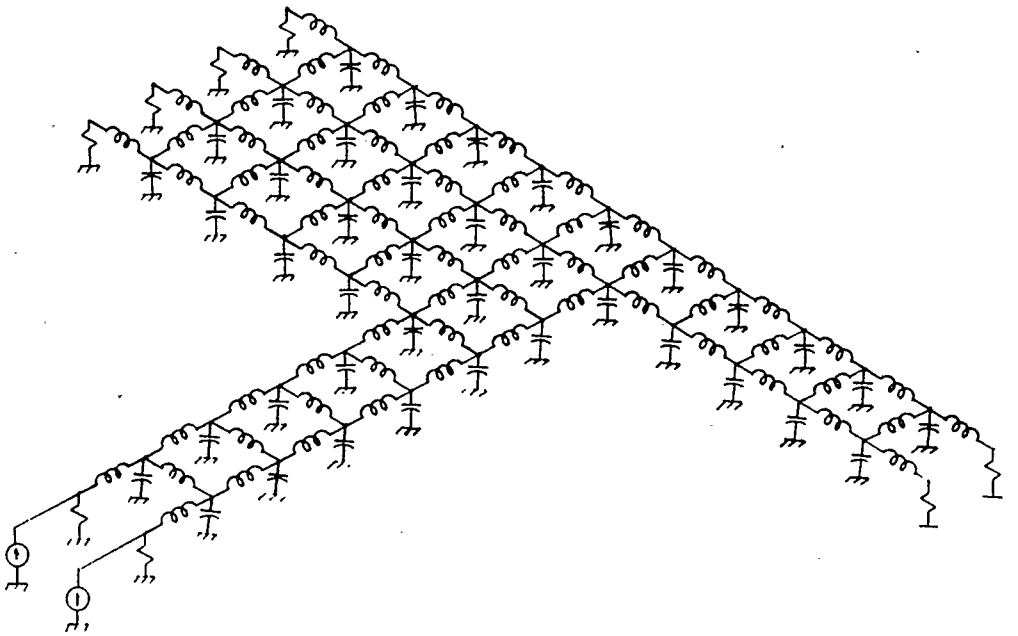

Figure 2.19 Equivalent circuit for a 25-50-50 and 20-50-50 Ω Tee

Fig. 2.19 shows the circuit used to calculate the scattering parameters for a 25-50-50 Ω Tee and a 20-50-50 Ω Tee. The number of nodes per width varies approximately inversely with the impedance of each line. Two nodes per width were used for the 50 Ω line. If three nodes per width were used the 20 or 25 Ω line would have 6 nodes per width, which would have slowed calculation considerably.

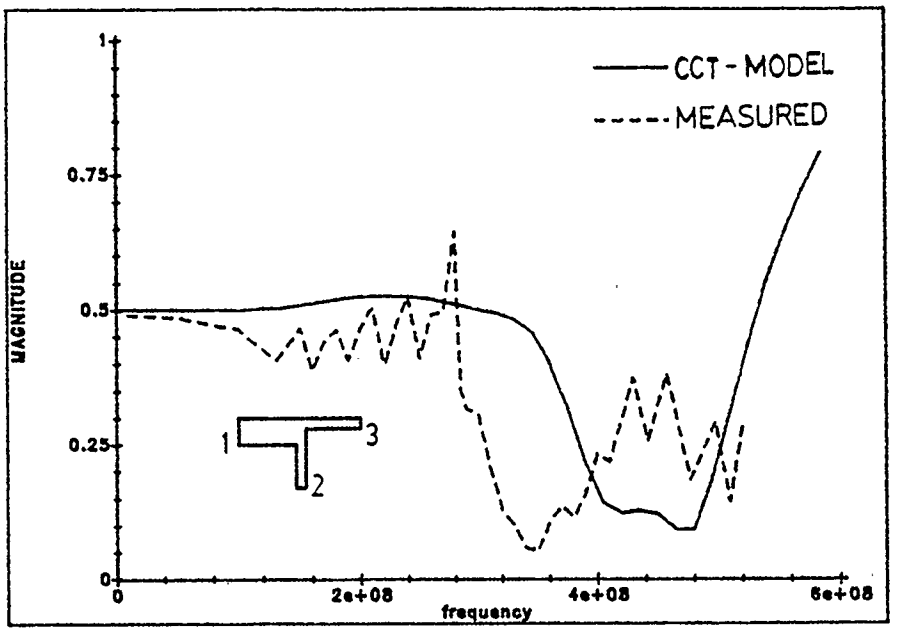

Figure 2.20 S_{22} of a 25-50-50 Ω Tee $\varepsilon_r = 2.32$ h=3.81 *cm*

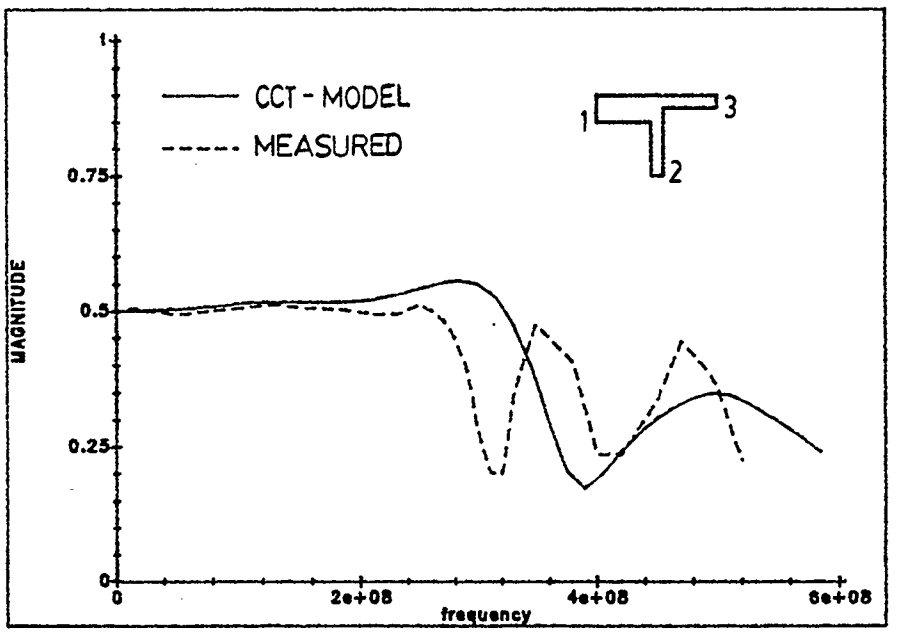

Figure 2.21 S_{32} of a 25-50-50 Ω Tee $\varepsilon_r = 2.32$ h=3.81 *cm*

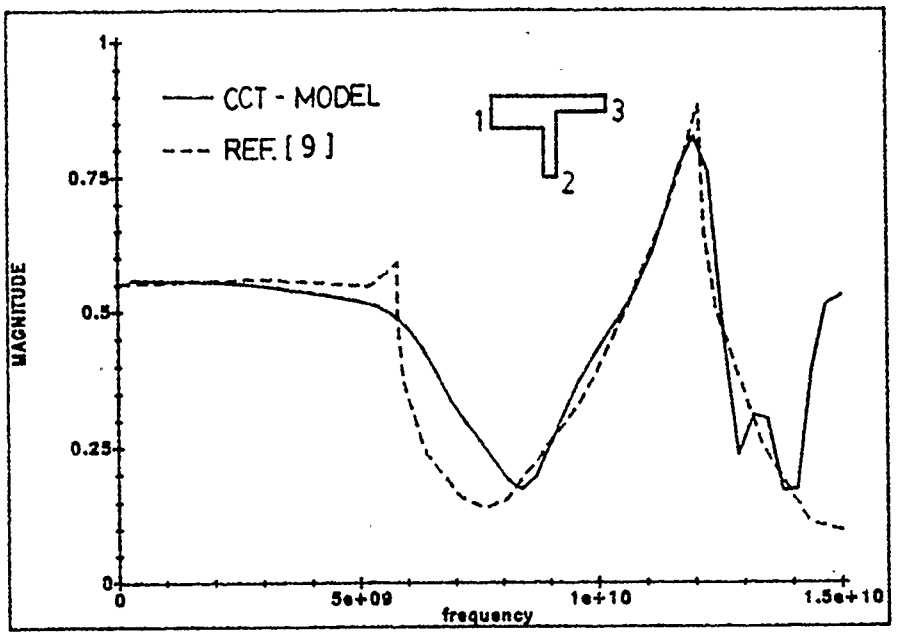

Figure 2.22 S_{22} of a 20-50-50 Ω Tee ε_r = 2.32 h=0.156 *cm*

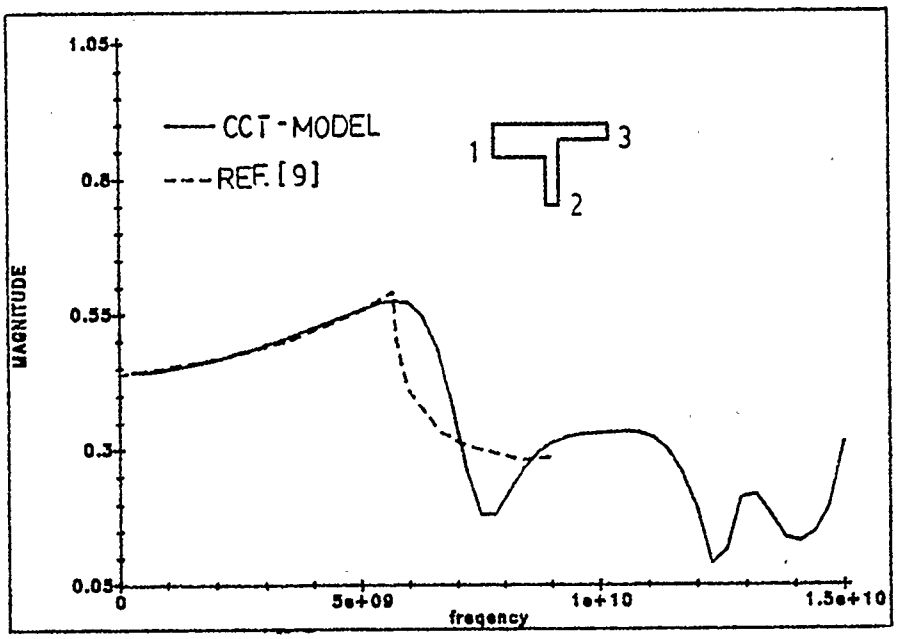

Figure 2.23 S_{32} of a 20-50-50 Ω Tee ε_r = 2.32 h=0.156 *cm*

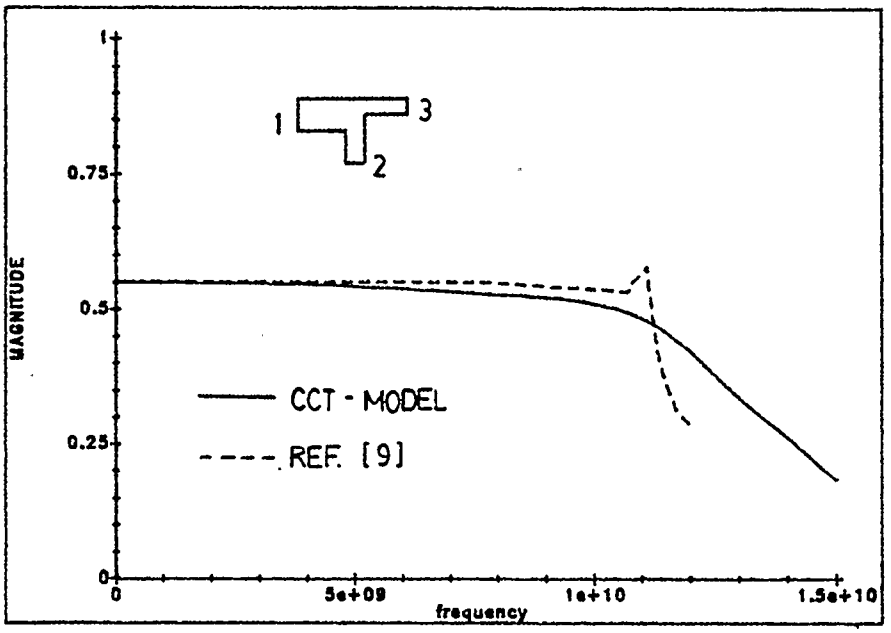

Figure 2.24 S_{22} of a 20-50-50 Ω Tee $\varepsilon_r = 2.32$ $h = 0.08$ *cm*

The circuit in Fig. 2.19 can be modified as shown in Fig. 2.25 to analyze another microstrip line configuration. Scattering parameters of this configuration are shown in Figs. 2.26 and 2.27

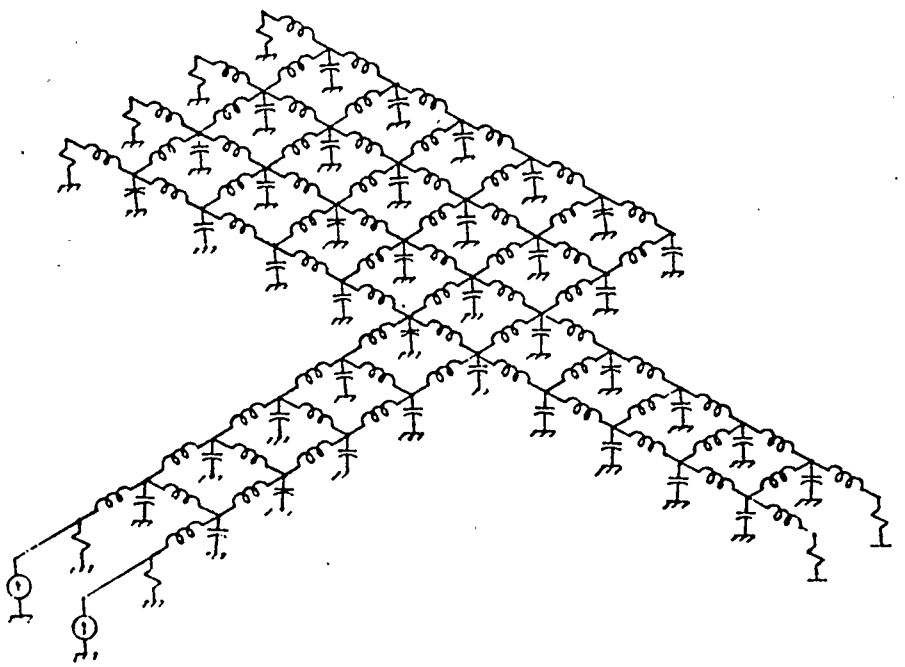

Figure 2.25 Equivalent Circuit for a 20-50-50 Ω Tee

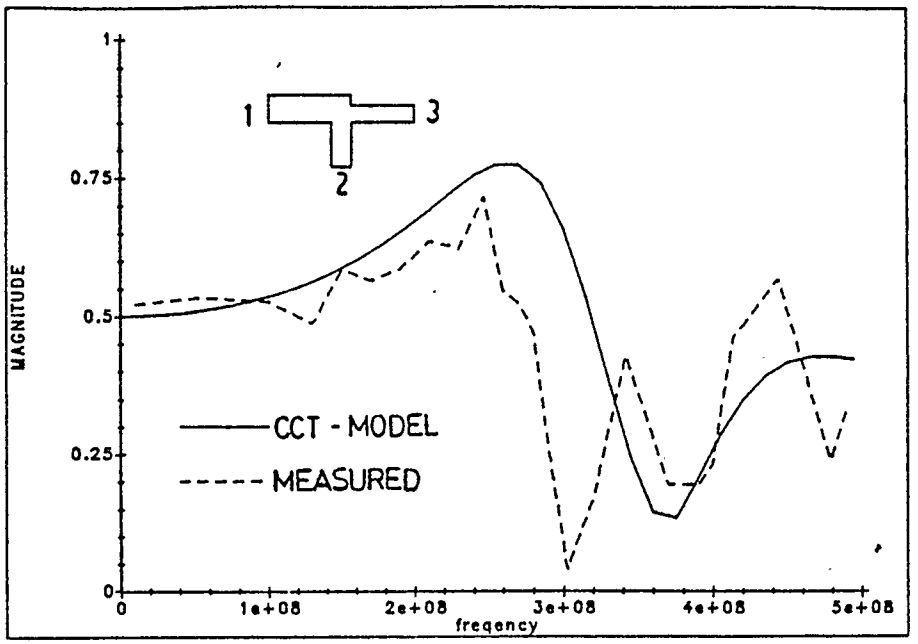

Figure 2.26 S_{22} of a 25-50-50 Ω Tee $\varepsilon_r = 2.32$ $h = 3.81$ *cm*

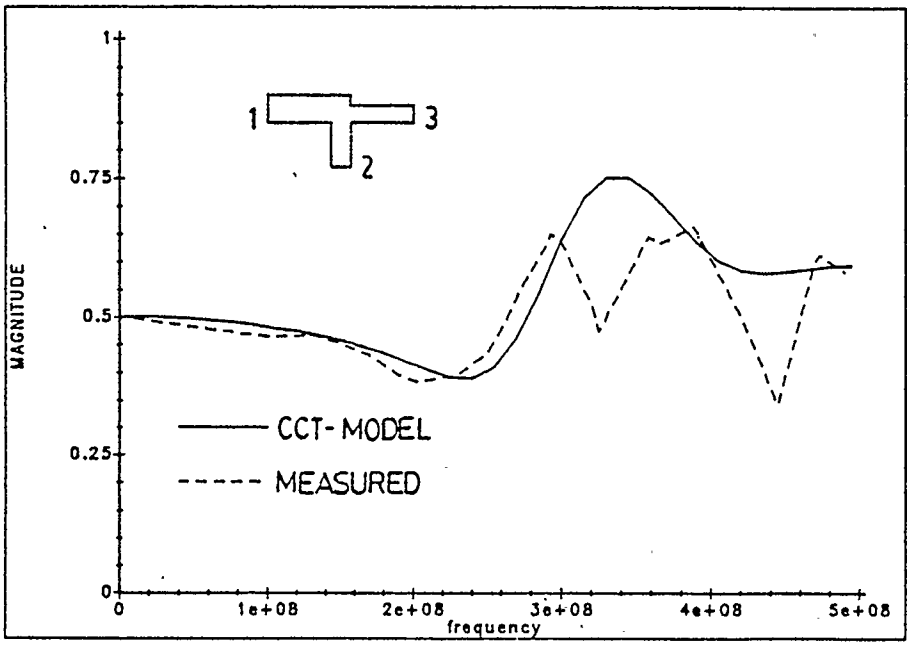

Figure 2.27 S_{32} of a 25-50-50 Ω Tee $\varepsilon_r = 2.32$ $h = 3.81$ *cm*

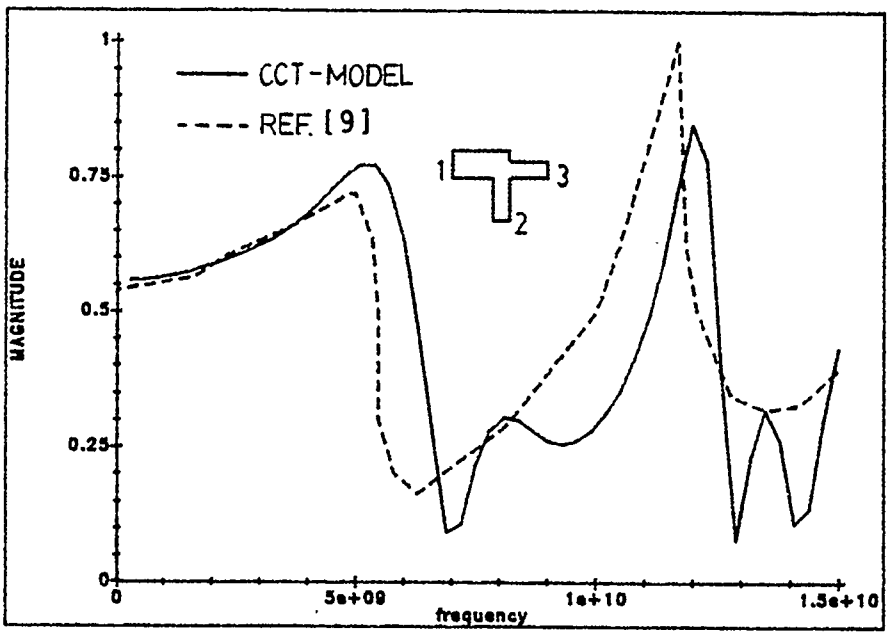

Figure 2.28 S_{22} of a 20-50-50 Ω Tee $\varepsilon_r = 2.32$ $h = 0.156$ *cm*

Similarly, sections of 2D-transmission line can be combined to form any discontinuity configuration with a Manhattan type geometry. For instance, Figs. 2.29 through 2.32 show scattering parameters, magnitude and phase, of two intersecting lines (cross). Figs. 2.33 through 2.36 show scattering parameters of various microstrip step discontinuities. To illustrate the usefulness of the circuit model developed in analyzing multiple discontinuities, scattering parameters of a double corner are shown in Figs. 2.37 and 2.38.

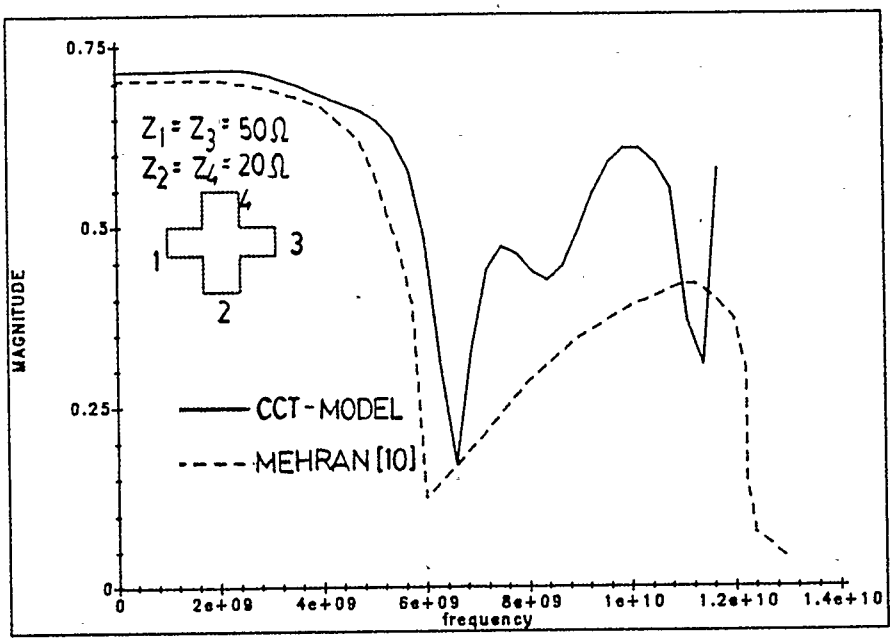

Figure 2.29 S_{11} for 50-20 Ω Cross $\varepsilon_r = 2.32$ $h = 0.156$ *cm.*

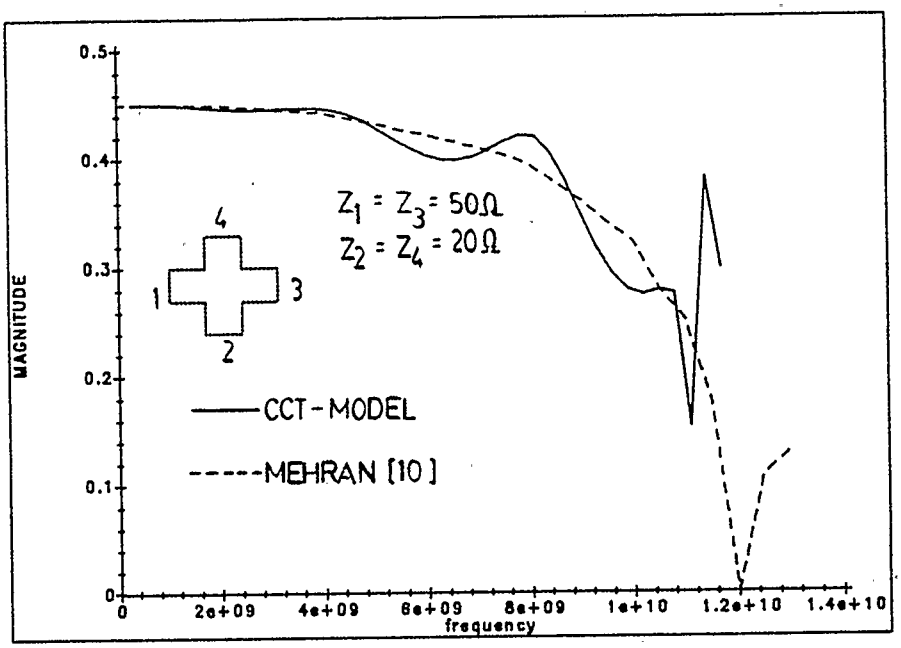

Figure 2.30 S_{21} for 50-20 Ω Cross $\varepsilon_r = 2.32$ $h = 0.156$ *cm.*

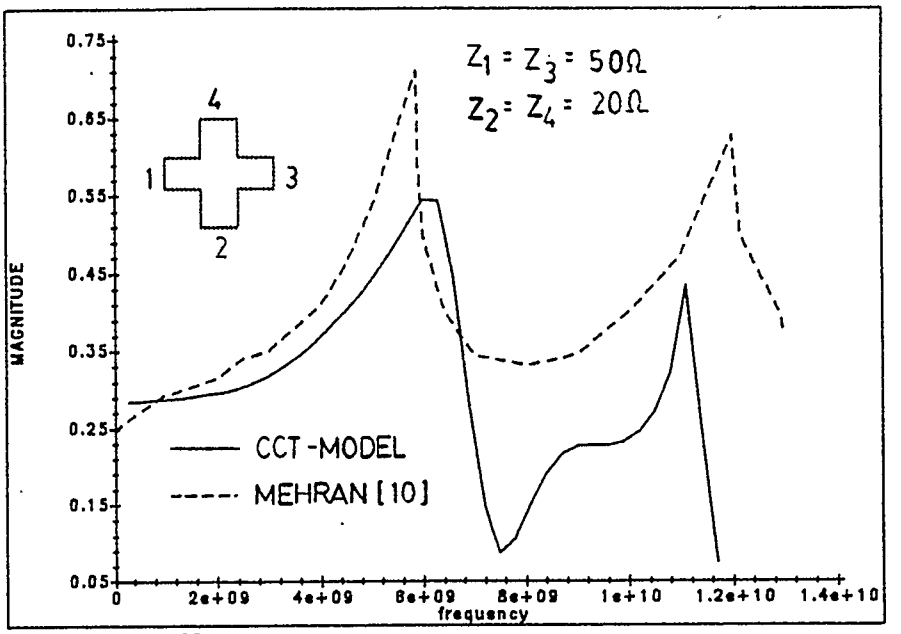

Figure 2.31 S_{31} for 50-20 Ω Cross $\varepsilon_r = 2.32$ $h = 0.156$ *cm.*

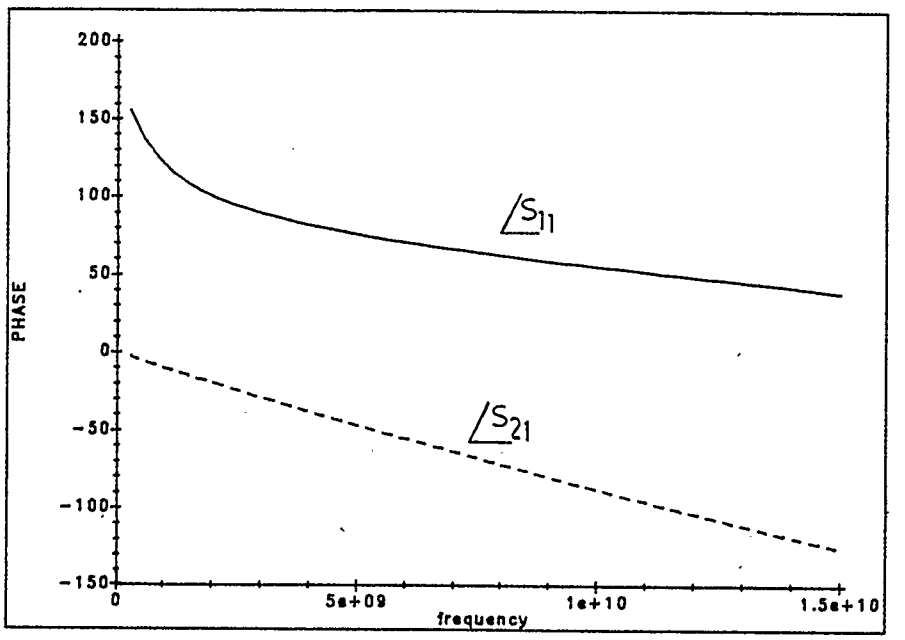

Figure 2.32 Phase of S_{11} and S_{21} for 50-20 Ω Cross $\varepsilon_r = 2.32$ $h = 0.156$ *cm.*

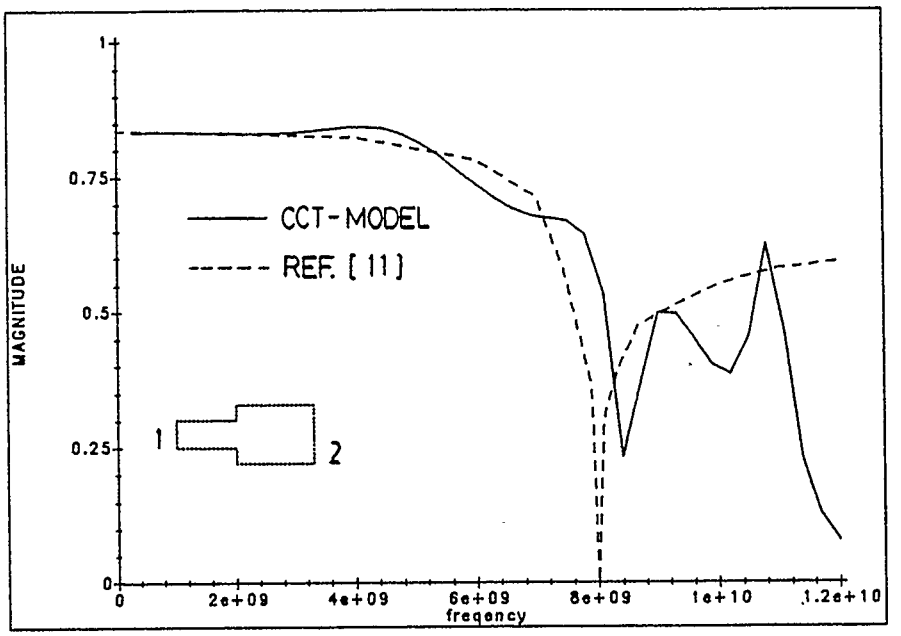

Figure 2.33 S_{21} for an Impedance Step $Z_1 = 50\Omega$ $Z_2 = 15\Omega$ $\varepsilon_r = 2.32$ $h = 0.156$ *cm.*

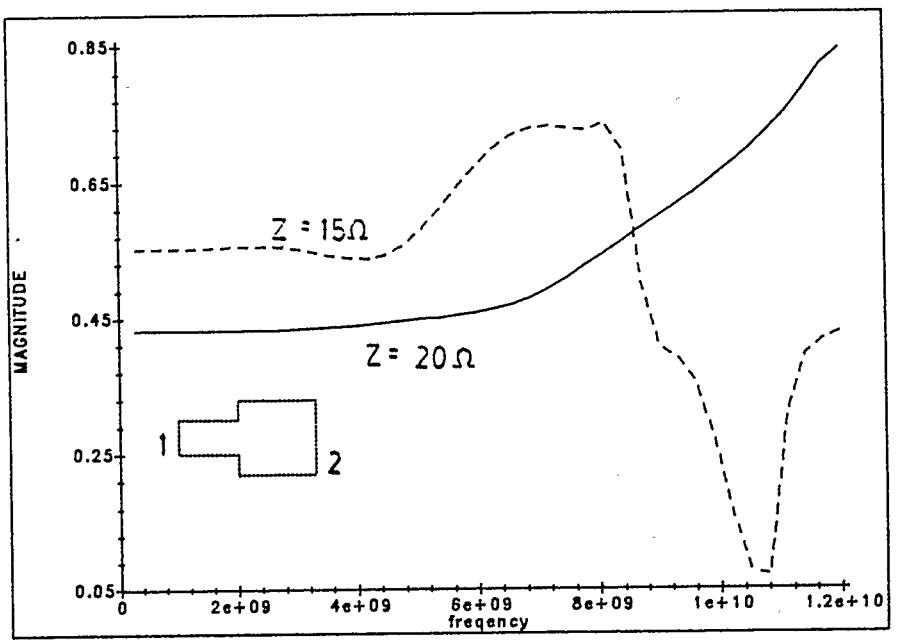

Figure 2.34 S_{11} for an Impedance Step $Z_1 = 50\Omega$ $Z_2 = 20$ and 15Ω $\varepsilon_r = 2.32$ $h = 0.156$ *cm.*

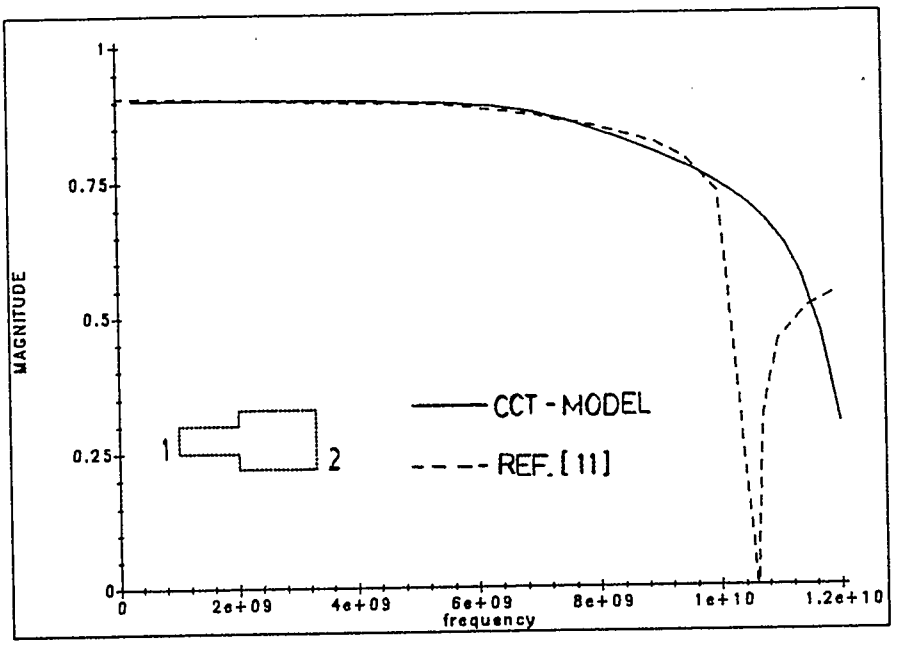

Figure 2.35 S_{21} for an Impedance Step $Z_1 = 50\ \Omega$ $Z_2 = 20\Omega$ $\varepsilon_r = 2.32$ $h = 0.156$ *cm.*

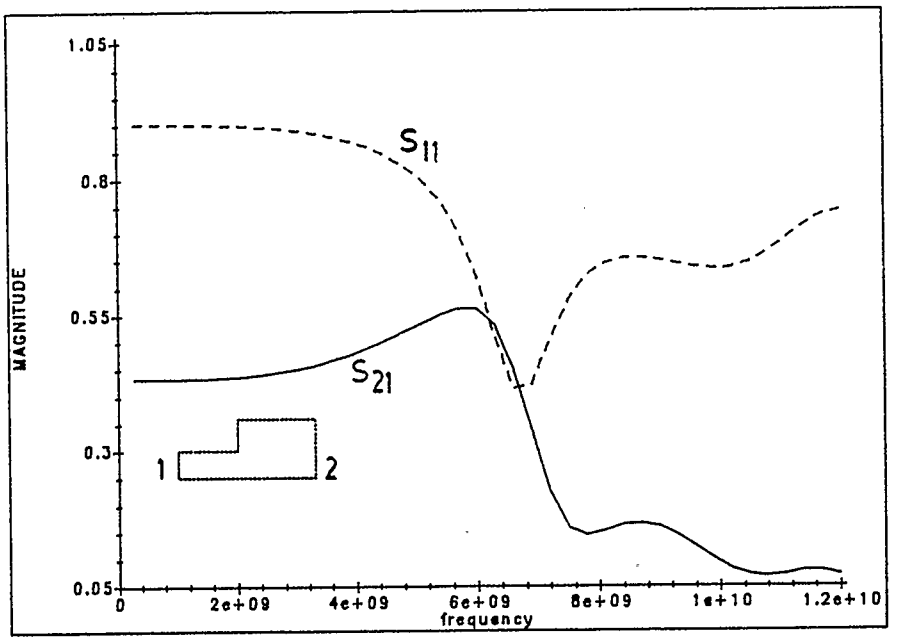

Figure 2.36 S_{11} and S_{21} for an Impedance Step $Z_1 = 50\Omega$ $Z_2 = 20\Omega$ $\varepsilon_r = 2.32$ $h = 0.156$ *cm.*

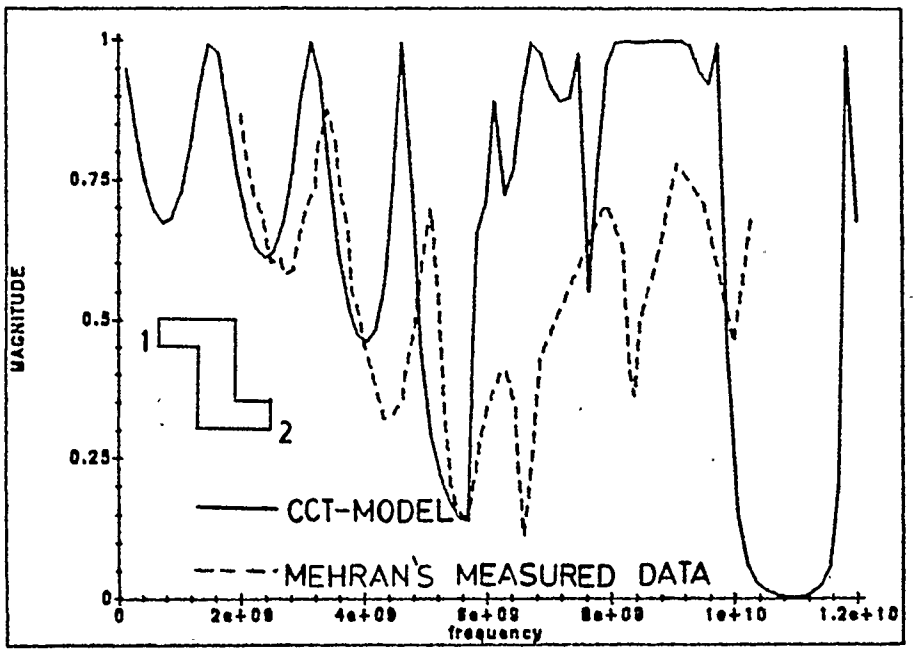

Figure 2.37 S_{21} for a 50–20–50Ω Double Corner $\varepsilon_r = 2.32$ $h = 0.156$ *cm.*

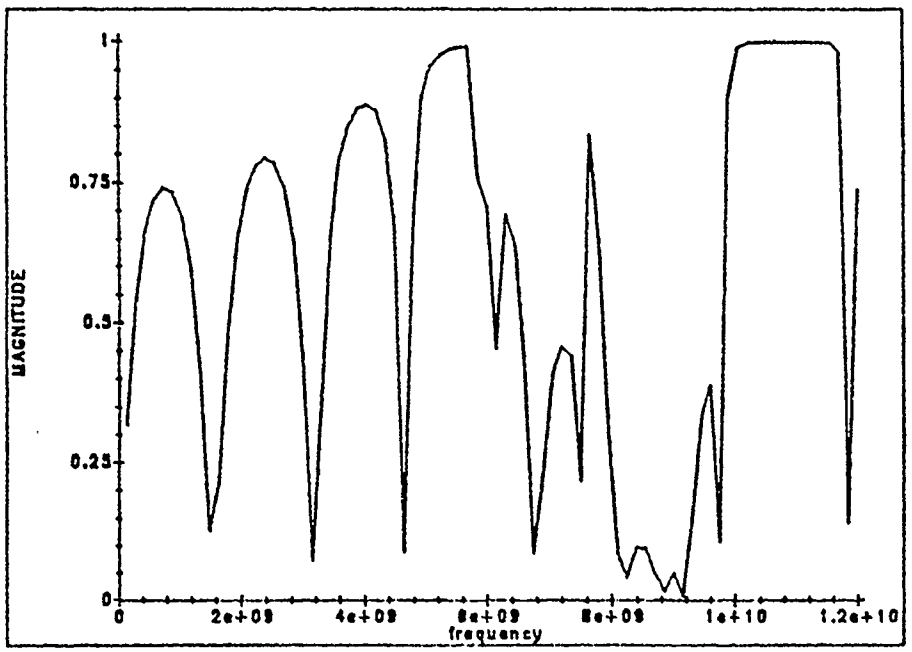

Figure 2.38 S_{11} for a 50–20–50Ω Double Corner $\varepsilon_r = 2.32$ $h = 0.156$ *cm.*

2.5. Observations

Figs. 2.8 through 2.38 show that the calculated results agree fairly well with experimental and published results. In some calculated results the cut-off frequency is higher than expected, in others the roll-off is too flat. The source of these discrepancies is subject to speculation. The small number of nodes per width results in reduced accuracy. Discrepancies in magnitude, particularly around the cut-off frequency can at least in part be attributed to radiation. Ripples in the measured results can be attributed to the fact that terminations are matched only for the *TEM* mode. Waveguide modes are subject to multiple reflections. This may lead to a considerable amount of error above the cut-off frequency of these modes.

In any microstrip circuit, propagation or reflection of waveguide modes depends not only on the discontinuity under consideration but on the entire circuit. That is, any mode may be reflected from, or generated in a neighboring discontinuity, and thus affect the scattering parameters of the discontinuity under consideration. Therefore an exact analysis would require that the entire microstrip circuit be analyzed simultaneously. This is rarely practical, and assumptions about termination of individual discontinuities must be made.

With these considerations in mind one can conclude that the results presented in this chapter are more than adequate for engineering purposes. The engineer is only concerned with discrete bands of frequencies. Allowing for a small margin of error, the design engineer can obtain all necessary information easily and reliably with the method presented here.

CHAPTER 3

THE SIGNIFICANCE OF TE MODES IN MICROSTRIP DISCONTINUITIES

3.1. Introduction

The method of determining scattering parameters developed in this thesis hinges on the assumption that substantially all the energy of a signal propagating in a microstrip is contained in the *TEM*-hybrid and one or more *TE* modes. In the previous chapter a model was developed that accounts for the *TEM* and a limited number of *TE* modes. While this model predicts the scattering parameters of the *TEM* mode adequately, no evidence was given that *TE* modes exist or that the *TE* modes contain the energy lost from the *TEM* modes. If *TE* modes are as significant as assumed in Chapter 2 a detailed analysis of the effects of the these modes is appropriate for two reasons.

1. Showing that the *TE* modes contain the balance of energy between the incident *TEM* wave and the reflected *TEM* waves will substantiate the theory put forth in Chapter 2. The difference between the incident *TEM* energy and the *TEM* energy leaving the discontinuity can be very substantial.

2. The *TE* modes can affect circuit operation. If a discontinuity whose incident wave is wholly in the form of a *TEM* mode can excite *TE* modes, one can speculate that another discontinuity may result in the transfer of energy from

TE modes back to the *TEM* mode. The presence of these modes may thus affect circuit operation considerably.

3.2. Waveguide Modes

The significance of the 2-D transmission line model is that the voltage may vary across the width of the conductor. As shown in Chapter 2, *TE* modes give rise to a cosinusoidal voltage distribution perpendicular to the direction of propagation. Since this voltage distribution constitutes a standing wave the equivalent circuit can be reduced to two parallel *TE* mode equivalent circuits. Specifically, in Chapter 2 it was shown that a two or three node per width equivalent circuit can be reduced to two parallel *TE* equivalent circuits.

In general, a microstrip line divided into n nodes per width can be used to model the first $n-1$ *TE* modes. An expression for voltage as a function of the lateral coordinate will be developed. This expression will permit calculation and measurement of the *TE* mode magnitude and phases. Comparing measured and calculated modal content will help to qualify the usefulness of the circuit model in predicting various modes.

The voltage at any point on the conductor is given by:

$$\vec{V}(y,z,t) = \vec{V}_{TEM}(z,t) + \vec{V}_{TE_{10}}(y,z,t) + \vec{V}_{TE_{20}}(y,z,t) \cdots \tag{3.1}$$

By limiting the frequency to a level well below the cut-off frequency of the highest mode considered, equation (3.1) can be truncated without introducing any significant error. It is a well known fact that each mode propagates with a

different speed.

$$\vec{E} = E_{TEM} e^{j\omega t - \gamma_{TEM} z} + \sum_{n=1}^{N} E_{TE_{no}} \cos\left[\frac{n\pi y}{w_{eff}}\right] e^{j\omega t - \gamma_{TE_{no}} z} \tag{3.2}$$

where $\gamma = \frac{\omega}{c}\sqrt{\varepsilon_{eff}}$ for *TEM* modes

and $\gamma = \left\{\left\{\frac{n\pi}{w_{eff}}\right\}^2 - \omega^2 \varepsilon_{eff}\right\}^{1/2}$ for *TE* modes.

and

$$\vec{V} = h\,\vec{E} \tag{3.3}$$

The time dependence is common to all modes and can thus be factored out. When all modes are observed at a particular value of z equation (3.2) becomes:

$$\vec{V}(z_1) = V_{TEM}\angle\Phi_o + V_{TE_{10}}\angle\Phi_1 \cos\left[\frac{\pi y}{W_{eff}}\right] + V_{TE_{20}}\angle\Phi_2 \cos\left[\frac{2\pi y}{W_{eff}}\right] \cdots \tag{3.4}$$

where Φ is the phase angle of the polar form of the voltage at each node.

$V(z_1)$ can be calculated and measured. Each node of the equivalent circuit represents one of n equal squares into which the microstrip conductor is subdivided. The total width of the strip is $\frac{1}{2}$, 1 , $\frac{3}{2}$ *or* 2 cycles of the TE_{10}, TE_{20}, TE_{30} and TE_{40} mode respectively. Each row of nodes of the equivalent circuit, perpendicular to the direction of propagation, samples the lateral voltage distribution on the conducting strip. Equilateral samples of an odd function

like equally spaced samples of an integral number of cycles of a sinusoid add up to zero. For this reason the sum of the *TE* voltages calculated at adjacent nodes across the strip is zero. Summing all node voltages for a particular value of z gives nV_{TEM}/Φ . For a circuit model with n nodes per width the nodes are located at $y = \frac{1w}{2n}$, $y = \frac{3w}{2n}$, $y = \frac{5w}{2n}$, $\cdots y = \frac{(2n-1)w}{2n}$. Hence, $n-1$ of n equations can be used to solve for $n-1$ unknown coefficients. For 5 nodes per width:

$$\begin{bmatrix} \vec{V}_{TEM} \\ \vec{V}_{TE_{10}} \\ \vec{V}_{TE_{20}} \\ \vec{V}_{TE_{30}} \\ \vec{V}_{TE_{40}} \end{bmatrix} = \begin{bmatrix} 1 & \cos(\frac{\pi}{10}) & \cos(\frac{2\pi}{10}) & \cos(\frac{3\pi}{10}) & \cos(\frac{4\pi}{10}) \\ 1 & \cos(\frac{3\pi}{10}) & \cos(\frac{6\pi}{10}) & \cos(\frac{9\pi}{10}) & \cos(\frac{12\pi}{10}) \\ 1 & 0 & -1 & 0 & 1 \\ 1 & \cos(\frac{7\pi}{10}) & \cos(\frac{14\pi}{10}) & \cos(\frac{21\pi}{10}) & \cos(\frac{28\pi}{10}) \\ 1 & \cos(\frac{9\pi}{10}) & \cos(\frac{18\pi}{10}) & \cos(\frac{27\pi}{10}) & \cos(\frac{36\pi}{10}) \end{bmatrix}^{-1} \times \begin{bmatrix} \vec{V}_1 \\ \vec{V}_2 \\ \vec{V}_3 \\ \vec{V}_4 \\ \vec{V}_5 \end{bmatrix} \quad (3.5)$$

where V_1, V_2, V_3, V_4 and V_5 are the node voltages of $V(z_1)$ at $y = \frac{1w}{10}$, $y = \frac{3w}{10}$, $y = \frac{5w}{10}$, $y = \frac{7w}{10}$ and $y = \frac{9w}{10}$ respectively.

3.3. Calculated & Measured TE Modes

All measurements and calculations presented in this chapter are made at the load side of a 50-25 Ω corner. The source is connected to the 50Ω leg of this corner. In Fig. 3.1 the calculated magnitudes of TE_{10}, TE_{20}, TE_{30} and TE_{40} are shown. Voltages were calculated at five points on the microstrip conductor using the methods of Chapter 2. From this data the *TE* modes were found using

equation (3.5). Since the TE_{40} mode, as expected, does not exist in the frequency range considered, no truncation error is introduced. Calculation and measurements are made far enough from the discontinuity for evanescent modes to be heavily attenuated. Magnitudes of each mode should thus be constant with position, except for a small amount of attenuation. The phase of each mode varies with position according to equation (3.2).

In Figs. 3.2 through 3.4 calculated and measured *TE* modes are compared. The calculated and measured TE_{10} modes are very similar. The discrepancy in magnitude, as will be shown in Chapter 4, is expected due to radiation. The calculated TE_{20} mode exists in the same frequency band as the measured mode. However, the magnitude of the measured TE_{20} mode is much smaller.

Losses at high frequency are probably due mostly to radiation. There is no known theory for exact calculation of microstrip discontinuity radiation. The theories that have been developed assume pure *TEM* or quasi-*TEM* mode propagation. As will be explained in Chapter 4, for the *TEM* mode, radiation increases with the square of frequency. While there is no theory available for microstrip radiation due to waveguide modes, a clue to the frequency dependence of such radiation can be obtained from a related field. Patch antennas have a geometry and field distribution similar to microstrip discontinuities in which *TE* modes are excited. Fields excited by such an antenna increase directly with frequency, therefore, power radiated is proportional to the square of frequency. It is, thus, reasonable to assume that the frequency dependence of radiation from microstrip

discontinuities is the same for both, *TEM* and *TE* modes.

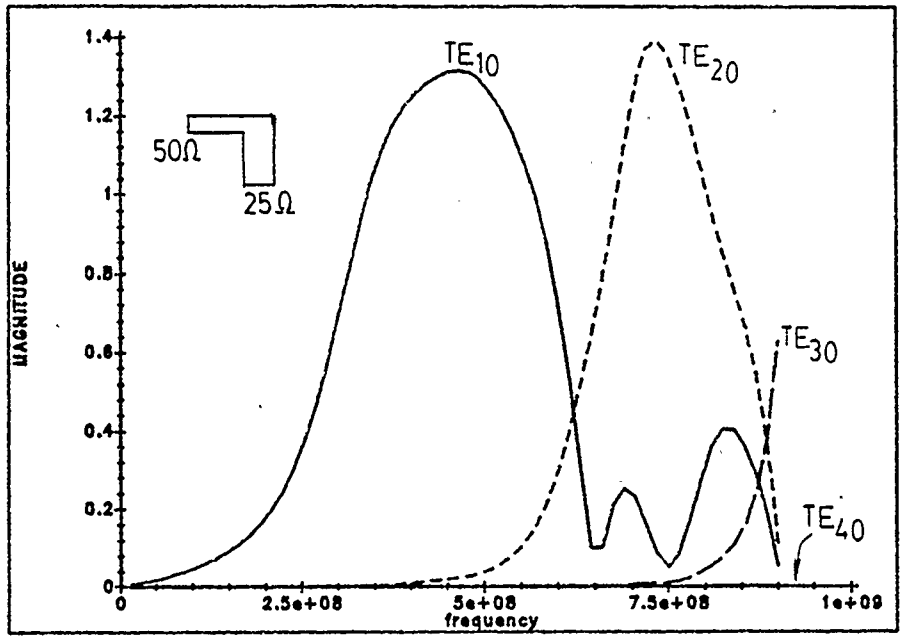

Figure 3.1 Calculated TE_{10}, TE_{20}, TE_{30} and TE_{40} modes.

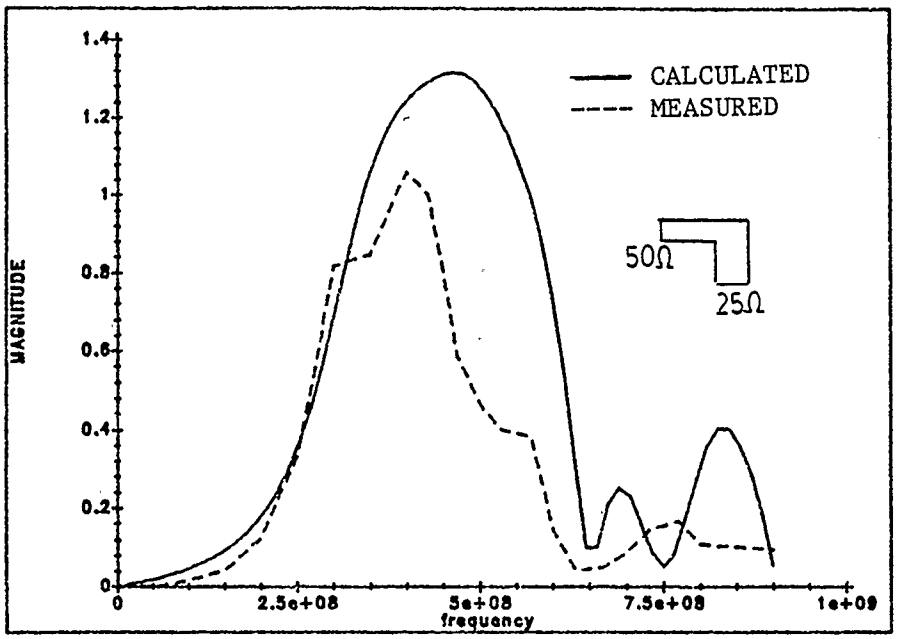

Figure 3.2 Comparison of calculated and measured TE_{10} modes.

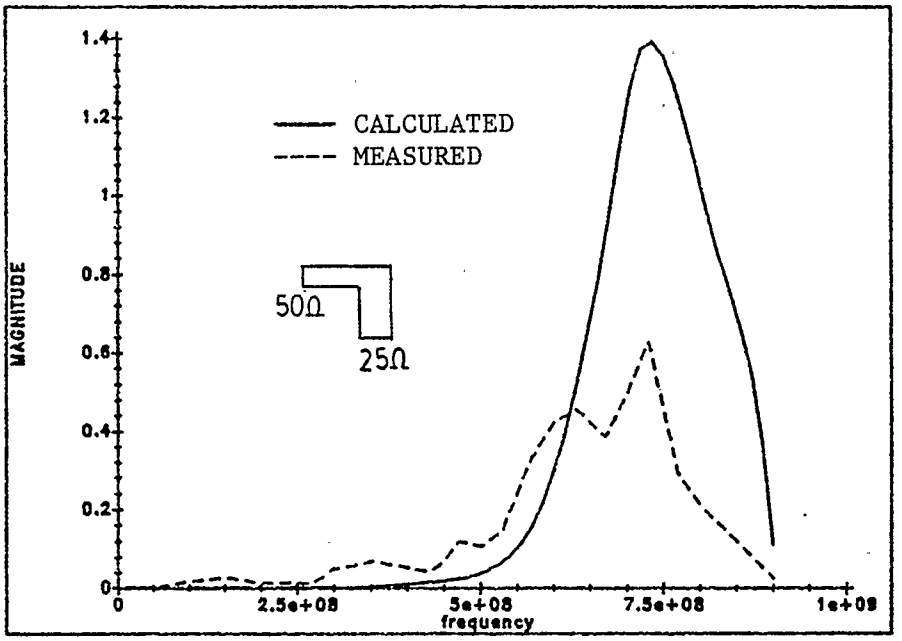

Figure 3.3 Comparison of calculated and measured TE_{20} modes.

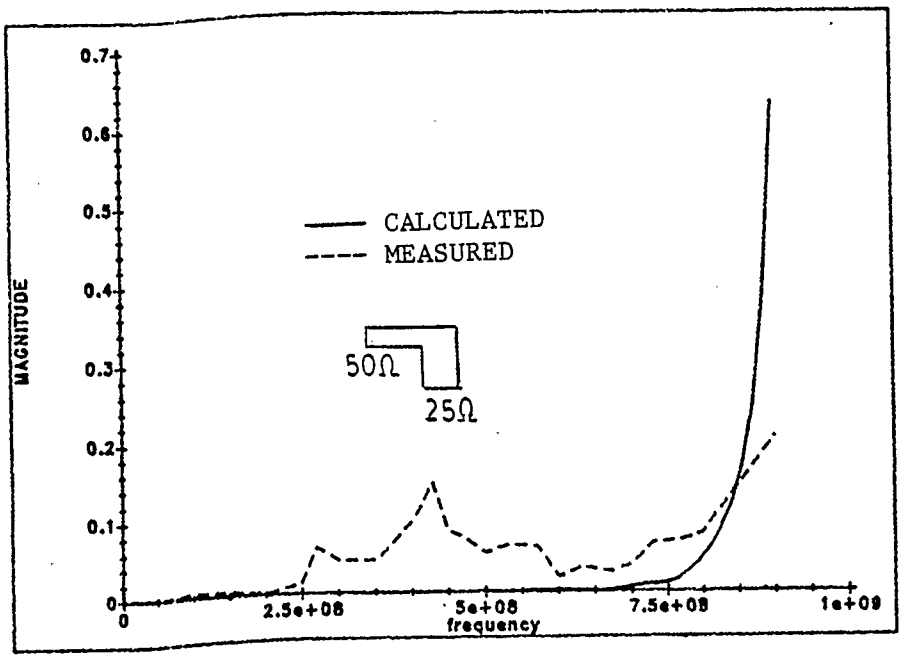

Figure 3.4 Comparison of calculated and measured TE_{30} modes.

It is to be noted, that the discrepancy in amplitude between the measured and calculated data for each of the modes (i.e. TEM, TE_{10}, TE_{20} etc.) increases as the order of the mode increases. This is consistent with the observation, that radiation increases with the square of frequency. Having justified the discrepancy between measured and calculated TE modes, one can conclude that the circuit model of Chapter 2 accounts for the first $n-1$ TE modes. While the foregoing analysis does not provide rigorous proof, any scepticism should only concern the accuracy to which TE_{20} and higher order modes are predicted.

From an engineering point of view the model presented provides significant benefits. Predicting the TE_{10} mode alone, as has been established in the previous chapter, increases the useful frequency range of the model to twice that of any

quasi-*TEM* model. Beyond that, higher order modes (TE_{20} and up) can be approximated. Exact calculation must include radiation losses because radiation alters microstrip performance significantly at frequencies where TE_{20} and higher order modes exist.

3.4. Effects of the TE Modes on Circuit Operation

So far it has been shown that in some discontinuities energy is coupled to *TE* modes. More specifically, the transmission coefficients, or S_{21} parameter in the example given, depend on the *TE* propagation characteristics.

In this section attention is focused on the circuit wide effect of *TE* modes. Given that *TE* modes exist, it is of considerable interest to know how will these modes affect circuit operation beyond their point of excitation. Knowing that a microstrip discontinuity can generate waveguide modes that contain a significant portion of the energy contained in the propagating signal, it seems obvious that an adjacent discontinuity can reverse this process. The author is not aware of any work published that concerns itself with the above consideration. Most publications deal with scattering parameters of the *TEM* mode without explicitly dealing with other modes excited. All modes which carry any significant amount of energy should be dealt with, as the following simulation will show.

To illustrate the importance of considering higher order modes, the scattering parameters of three microstrip components will be analysed. Fig. 3.5(a) shows a component with two planes of symmetry. If the component is split by the vertical

plane, the component becomes two cascaded impedance steps. The second impedance discontinuity can be reoriented to give the component of Fig. 3.5(b), a shunting stub. If the *TEM* wave coupling between the two discontinuities is the only coupling, the scattering parameters of this new component would not be altered from those of the first component. Now if the horizontal plane of symmetry is considered in Fig. 3.5(a) the component now consists of two cascaded right angle corners with an impedance step. If the second corner is reoriented we obtain the component shown in Fig. 3.5(c). Again, the scattering parameters of this component should be unchanged if higher order modes were not a factor. The scattering parameters of these three components are shown in Figs. 3.6(a) and 3.6(b).

The scattering parameters are similar at low frequencies and diverge rapidly at high frequencies until very substantial differences exist. Therefore higher order modes must be considered in discontinuities in close proximity. Microstrip circuits often consist of groups of discontinuities. Due to the strong dependence of microstrip lines on frequency, reflections at discontinuities can be very significant. Reflections in a circuit with two or more discontinuities result in a chain of events. Reflected waves are partially reflected and partially transmitted by adjacent discontinuities. Waves are, thus, bounced back and forth within a series of discontinuities resulting in a complex phasor adding and cancellation of numerous wave fronts.

This already complex form of propagation is considerably complicated when slab waveguide modes are present. Aside from having *TEM*, TE_{10} and higher order *TE* modes each with different impedance characteristics propagating between discontinuities, coupling between the two types of modes may also occur at each discontinuity.

Under these circumstances *TEM* scattering parameters of individual discontinuities are of limited use. However, an equivalent circuit can be constructed for a small group of discontinuities in close proximity according to the rules given in Chapter 2 (see Fig. 2.37). Such a circuit implicitly takes care of intermodal coupling, repeated reflections and all boundary conditions that exist at each discontinuity. Unlike with other methods of analysis, using this circuit model does not increase in difficulty as the strip configuration becomes more complex.

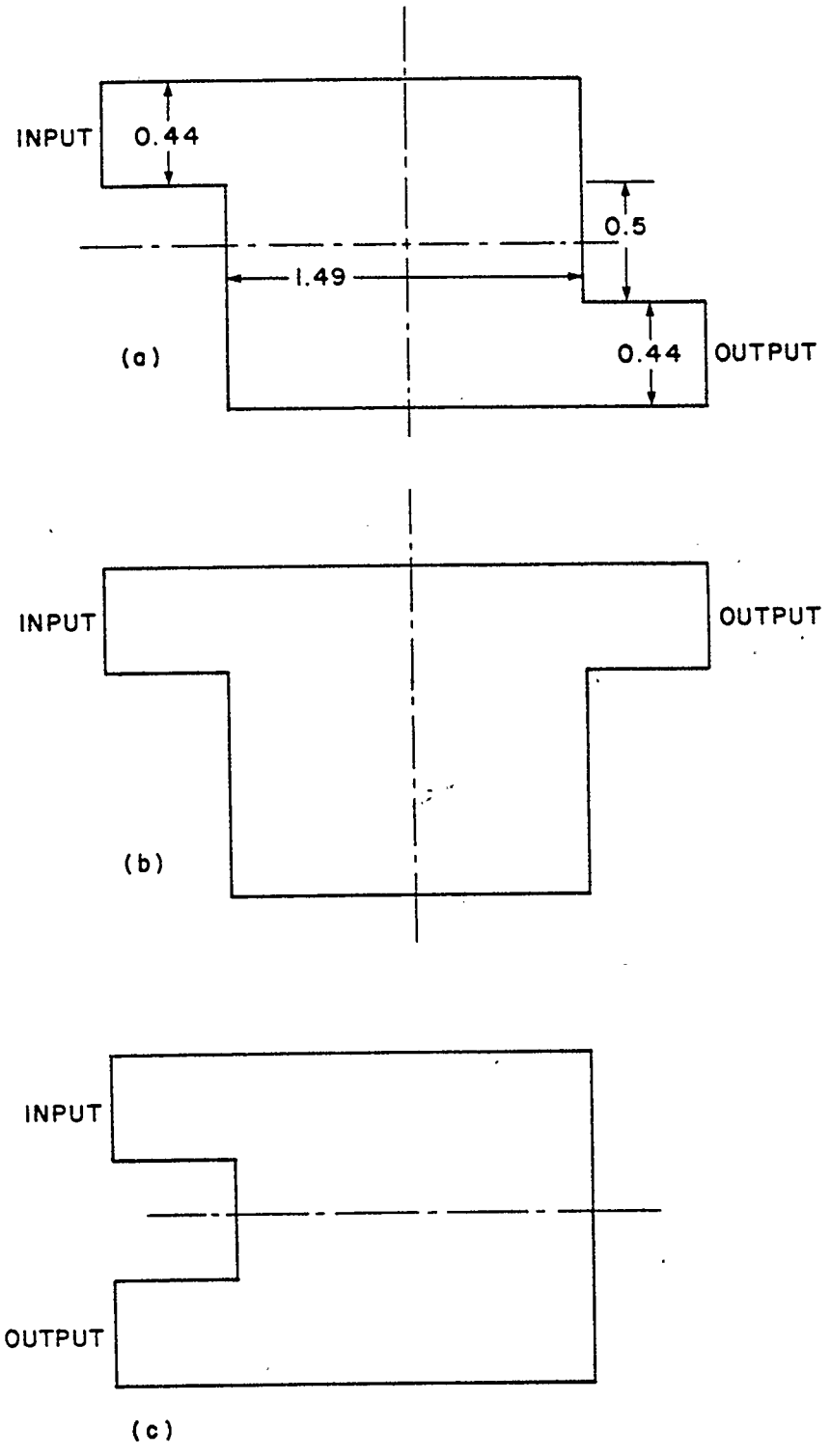

Figure 3.5 Three Microstrip Components

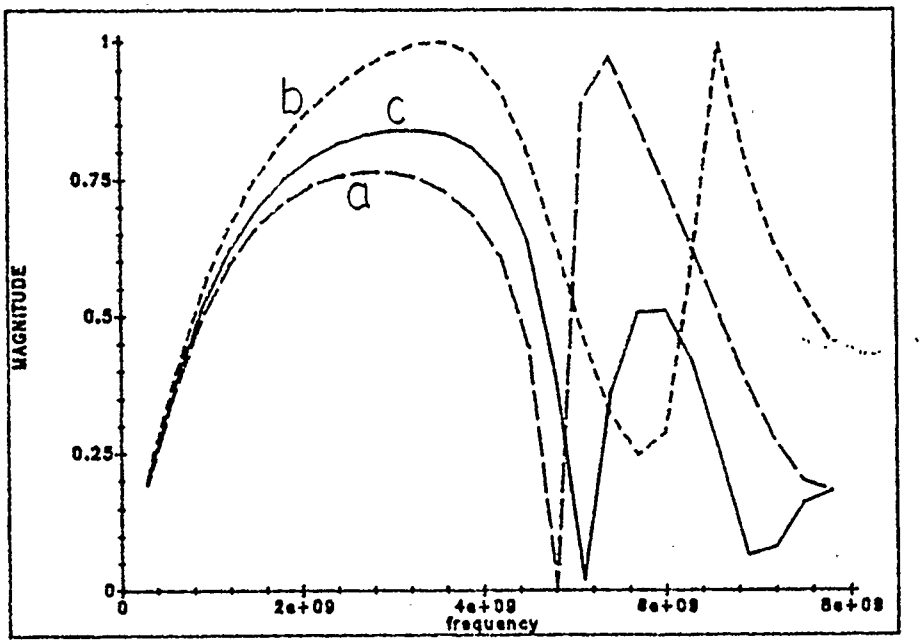

Figure 3.6a S_{11} For components a, b and c of Figure 3.1.

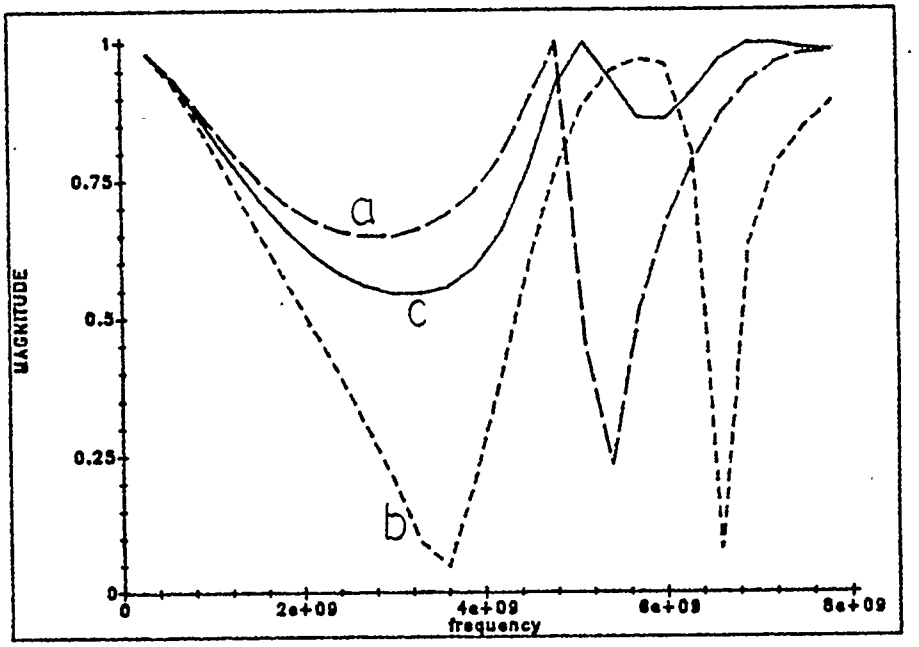

Figure 3.6b S_{21} For components a, b and c of Figure 3.1.

CHAPTER 4

RADIATION LOSSES IN MICROSTRIP DISCONTINUITIES

4.1. Losses in Microstrip Lines

In this chapter the equivalent circuit for microstrip discontinuities will be modified such that radiation losses can be included in the model. In microstrip lines energy is lost in a number of ways such as, radiation losses, resistive losses in the conductor and ground plate, dielectric losses and losses through the launching of substrate surface waves.

The resistivity of the conductor in microstrip lines depends on the skin depth and current distribution. Discontinuities have only a second order effect on conductor and dielectric losses while they change the current distribution on the conductor and dielectric of the microstrip line. This type of loss is therefore not pursued in any more detail here. Theory for predicting energy lost to substrate surface waves is only partially successful. For this reason laboratory measurements were used to obtain an estimate for the amount of energy lost to surface waves. As will be shown later in this chapter, these losses are small compared to radiation losses.

Radiation is directly caused by a redirection of current flow as imposed by the microstrip discontinuity geometry. This type of loss is therefore in context with the subject of this thesis. Furthermore, radiation increases with the square of frequency, microstrip circuit performance is thus affected more severely at high

frequencies. Radiation may even limit the useful frequency range of operation for some microstrip lines. For these reasons it is very desirable to be able to model radiation losses.

4.2. Radiation From Microstrip Open Circuits

A microstrip discontinuity always involves a change in current direction either for part or all of the current on the strip. All discontinuities, therefore, lose some energy through radiation. There is no known theory for exact calculation of microstrip radiation. The complex mode distribution in discontinuities called for simplifying assumptions in the analyses. All analyses presented here assume only the *TEM* or quasi - *TEM* mode is present in the strip.

Lewin [12] was perhaps the first to analyze radiation from microstrip discontinuities. Lewin used the strip current, the component $(\varepsilon_r - 1)$ of the displacement current and their images in the ground plane to find the magnetic vector potential. Using equations (4.1) and (4.2) he calculates the electric field and the power radiated respectively.

$$\vec{E} = \frac{\nabla\nabla\cdot\vec{A}}{j\omega\varepsilon\mu} - j\omega\vec{A} \tag{4.1}$$

$$P = \int_S \frac{|\vec{E}|^2}{\eta_o}\, dS \tag{4.2}$$

where S denotes a closed surface.

From the expression of radiated power an equivalent conductance G_r can be deduced for unity incident current.

$$G_r = 60\left\{kt\right\}^2 F_1(\varepsilon_{eff}) \tag{4.3}$$

F_1 is called the form factor. In Equation (4.3) one configuration is distinguished from another through the form factor. That is, if a corner and a Tee with the same impedance lines and substrate types are considered, only the form factor will change in Equation (4.3) from the first analysis to the second.

Sobol [13] treated the end of a microstrip open circuit as an aperture to derive the radiation conductance given in Equation (4.4)

$$G_r = \frac{\sqrt{\varepsilon_{eff}}}{240\pi^2} F_2(\sqrt{\varepsilon_{eff}}\frac{2\pi w}{\lambda_o}) \tag{4.4}$$

$$F_2(x) = x\, Si(x) - 2\sin^2(\frac{x}{2}) - 1 + \frac{\sin x}{x} \tag{4.5}$$

The radiation conductance used for radiation calculation in this chapter was derived by James and Henderson [14] and is given in Equation (4.6)

$$G_r = \frac{4\pi h w_{eff}}{3\lambda_o^2\sqrt{\varepsilon_{eff}}Z_o} \tag{4.6}$$

and this can be simplified to

$$G_r = \frac{f^2 w_{eff}^2}{90c^2} \tag{4.7}$$

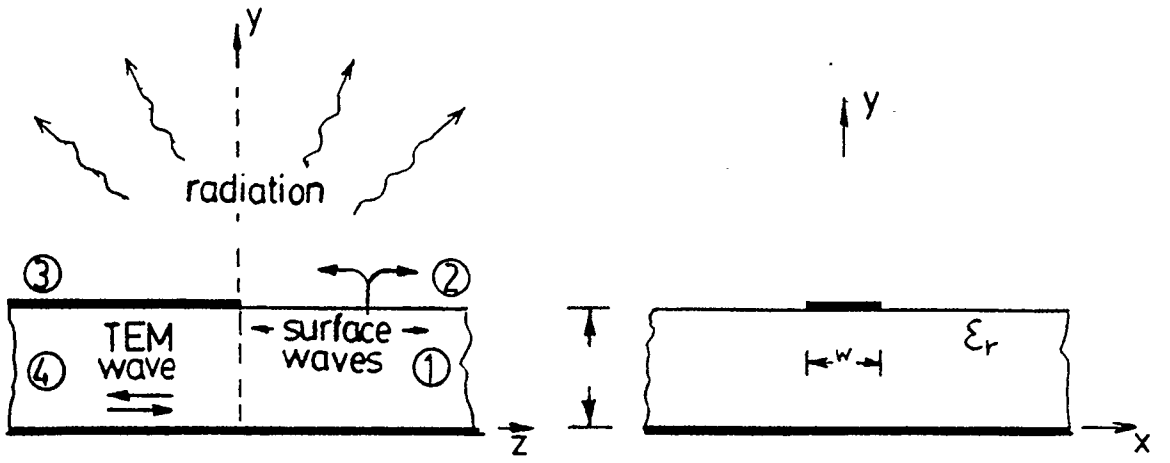

Figure 4.1 Sectional diagram of microstrip termination

James and Henderson subdivided the microstrip termination into four regions as shown in Figs. 4.1. For regions 1 and 2 the Hertzian electric and magnetic vector potential is formulated for surface waves and radiation fields. For region 4 the fields are assumed to be quasi *TEM*. In region 3 the electric and magnetic fields are assumed to be zero. In this analysis a vertical aperture A in the (*xy*0) plane is defined as the boundary of these regions. The fields in region 3 are a function of the reflection coefficient Γ. Once Γ is evaluated by solving for the fields in the four regions G_r can be determined using:

$$YZ_o = \frac{(1-\Gamma)}{(1+\Gamma)} = (G_r + G_s + j\omega\beta)Z_o \tag{4.8}$$

Wood, Hall and James [15] succeeded in measuring the end admittance of an open circuit microstrip line. With equipment specifically built for the task, they measured the VSWR of the line. The end admittance is given by

$$G_r = \frac{S}{Z_o(S^2\cos^2\left\{\frac{\Phi}{2}\right\} + \sin^2\left\{\frac{\Phi}{2}\right\})} \tag{4.9}$$

$$B = \frac{(S^2 - 1)\sin\left\{\frac{\Phi}{2}\right\}\cos\left\{\frac{\Phi}{2}\right\}}{Z_o(S^2\cos^2\left\{\frac{\Phi}{2}\right\} + \sin^2\left\{\frac{\Phi}{2}\right\})} \tag{4.10}$$

Where S is the VSWR and Φ is the angular shift in the null position from that of an ideal open circuit. Wood et al compared Lewin's, Sobol's, James and Henderson's and other radiation conductances to their own measurements to establish the validity of each expression.

Despite the vast differences in approach of each analysis discussed above, the outcomes are very similar. In each expression the radiation conductance varies with the square of frequency. Sobol's and James and Henderson's analyses give excellent agreement with Wood et al's measured results. James and Henderson's analytical end conductance consists of two parts $G = G_r + G_s$. G_r is the component of the end conductance due to radiation and G_s accounts for energy launched in form of a surface wave. Their G_r agrees closely with Lewin's radiation conductance. From these observations it seems that Lewin's and James and Henderson's radiation conductances are the more accurate ones. Sobol's predicted radiation losses are approximately equal to the total losses due to radiation and substrate surface waves.

4.3. Equivalent Circuit Modification

A microstrip open circuit is not a true open circuit, but has a finite conductance and capacitive susceptance. The susceptance is due to the open structure that introduces additional capacitance to ground. The conductance is due to energy leaving the open circuit in form of radiation and surface waves. The effect of energy leaving the open circuit through radiation or surface waves on scattering parameters, is largely indistinguishable from that of a resistive load. Hence this form of energy loss can be modeled in the equivalent circuit by connecting a conductance, as derived in section 4.2, as a load.

Radiation is not limited to open circuits. In fact, any microstrip discontinuity causes a change in the direction of current flow, and thus some energy is lost to radiation. For discontinuities with 2 or more ports, it is not sufficient to know just the total amount of energy radiated. It is much more useful to know how individual scattering parameters are affected by radiation. The effect of radiation on individual scattering parameters has a bearing on circuit operation, and it is therefore the preferred way of representing radiation losses.

Radiation arises due to a change in current direction. To reflect this property in an equivalent circuit, the radiation conductance given in section 4.2 must be converted to a series resistance. To further illustrate the necessity of using a series resistance instead of a shunt conductance consider the discontinuity in Fig. 4.2.

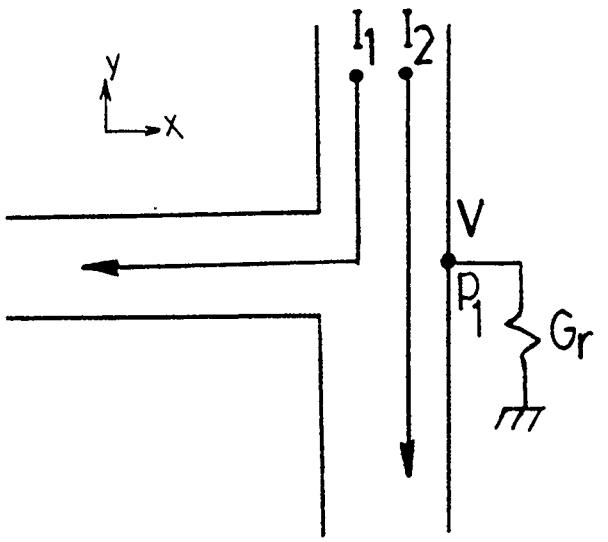

Figure 4.2 Effect of current direction on radiation.

Either current I_1 or I_2, not necessarily of the same magnitude, can give rise to the voltage V. Only current I_1 causes the discontinuity to radiate. A conductance at p_1 would dissipate the same amount of power if I_1 or I_2 is present. A series resistance placed parallel to the x-direction would only dissipate energy if I_1 is flowing.

This conversion from conductance to series resistance is first derived for a microstrip open circuit termination and will later be extended to other discontinuities.

First consider the *TEM* equivalent circuit of a transmission line terminated in an open circuit Fig. 4.3.

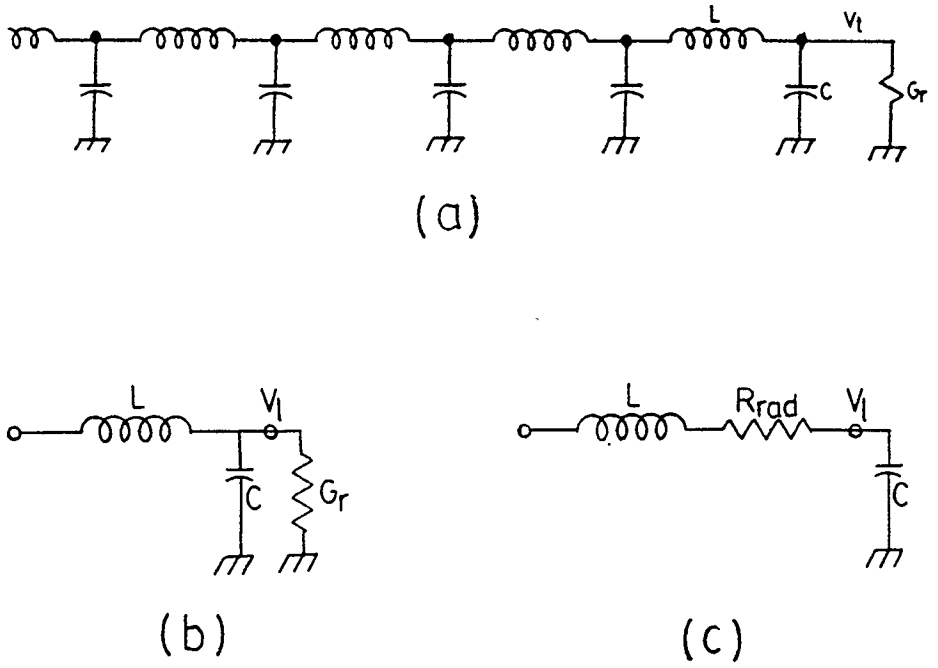

Figure 4.3 Equivalent circuit of open circuited microstrip line.

Figs. 4.3(b) and 4.3(c) both represent the last node of the equivalent circuit of Fig. 4.3(a). Formulating the input impedance for both circuits of Figs. 4.3(b) and 4.3(c) and equating the real part, R_{rad} can be derived from equation (4.7).

$$R_{rad} = \frac{h}{3\pi(\varepsilon_{eff})^{3/2} w_{eff}} \tag{4.11}$$

Next consider the 2D-equivalent circuit for open circuit terminated line;

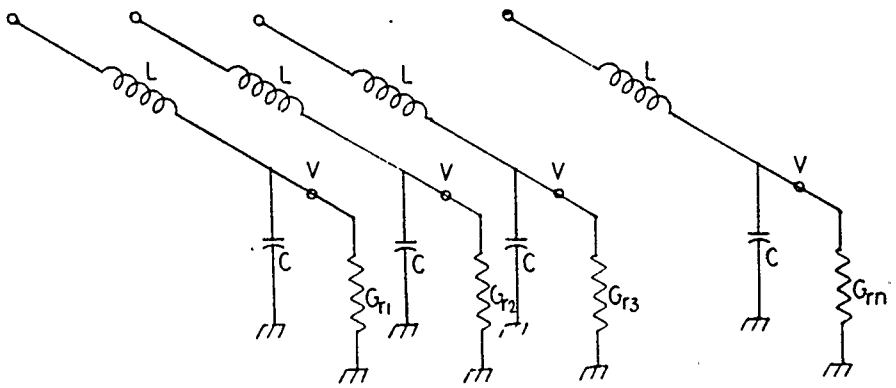

Figure 4.4 Conductance in 2D-transmission line model.

The voltage V and power radiated V^2G_r must be independent of the number of nodes the circuit is divided into.

$$P = V^2 \frac{G_{r1}}{n} + V^2 \frac{G_{r2}}{n} + \cdots + V^2 \frac{G_{rn}}{n} \tag{4.12}$$

$$P = V^2 G_r \tag{4.13}$$

$$\textit{since} \qquad G_{r1} = G_{r2} = \cdots = G_{rn}$$

and

$$R_{rad} = \frac{n^3 h}{3\pi(\varepsilon_{eff})^{3/2} w_{eff}} \tag{4.14}$$

Radiation can be modeled for all discontinuities considered in Chapter 2 and any other discontinuity possessing a Manhattan type geometry, by placing radiation resistances into the equivalent circuit. Radiation resistances are placed in the circuit similar to those in the open circuit between the last two rows of nodes of any line ending in a discontinuity (see examples).

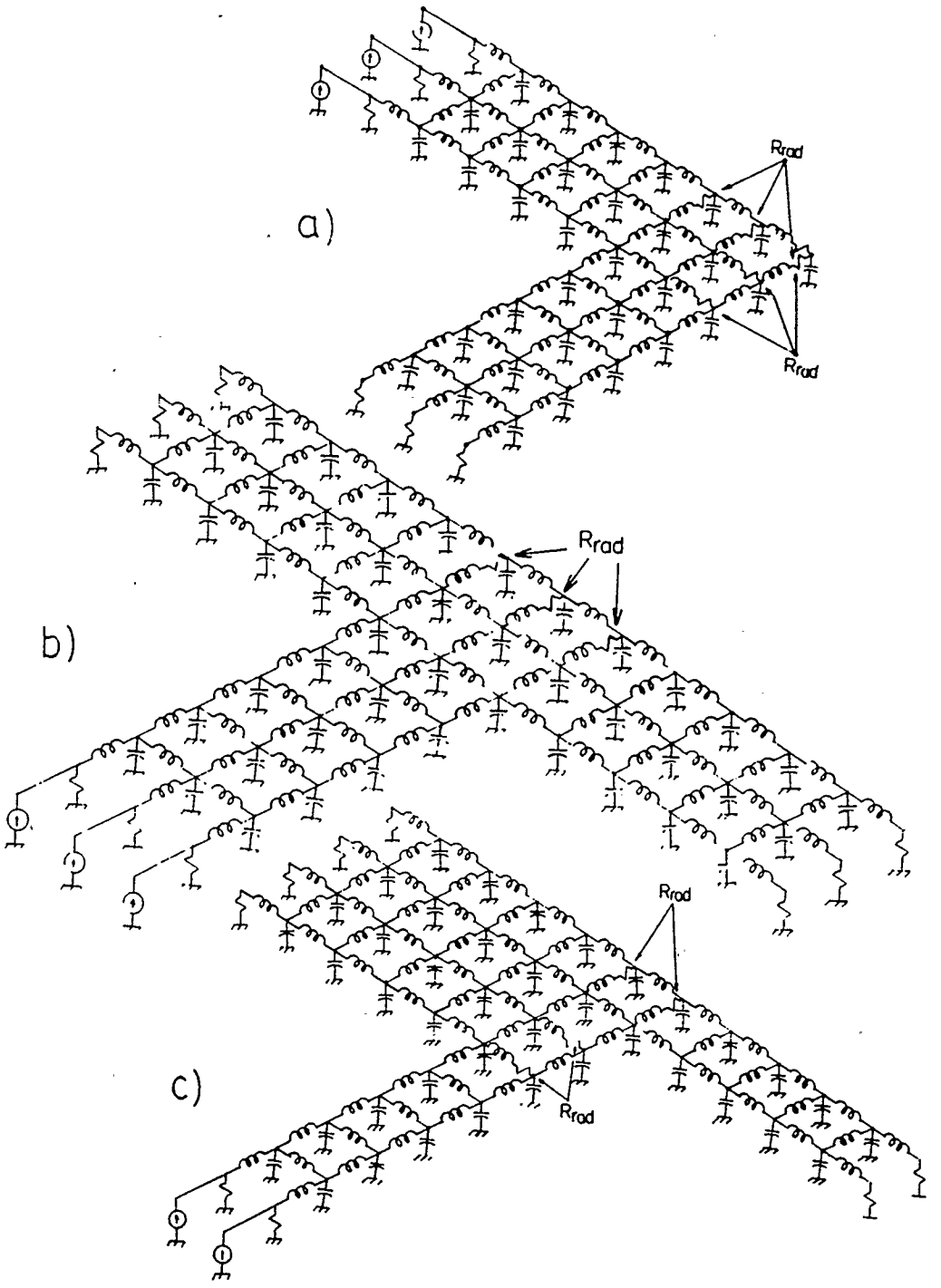

Figure 4.5 Examples of radiation resistances in various equivalent circuits.

The radiation resistance has been derived for a microstrip open circuit termination. The use of these resistances in other discontinuities will be justified for the

three most general cases: a corner, a symmetric Tee and a 90° branch. In the following analysis these discontinuities are compared to an open circuit in terms of voltages and current distribution. The results are compared to the analyses in Lewin's second paper on radiation [16] to qualify the approach presented.

4.3.1. 90° Corner

Scattering parameters of a corner in Fig. 4.9 show that at low frequencies all the incident energy is transmitted. For higher frequencies (0.65 GHz in the example of Fig. 4.9) all energy is reflected. Therefore we can think of a corner as a combination between a open and a matched termination. Representing a corner as a matched termination, Z_l in Fig. 4.6 is a frequency dependent load. For low frequencies $Z_l = Z_o$ and $V_l = V_{inc} = \frac{V_{oc}}{2}$, hence $\frac{1}{4}P_{oc}$ is radiated. For the case where all energy is transmitted the load side of the corner, with the exception of current direction, is identical to the the source side (see Fig. 4.6). For microstrips with large dielectric constants this is consistent with Lewin's analysis

$$F_{oc} = \frac{8}{3\,\varepsilon} \quad , \quad F_c = \frac{4}{3\,\varepsilon} \tag{4.15}$$

For the frequency at which all energy is reflected the source side of the corner is identical to an open circuit. No current flows in the leg on the load side, hence the whole circuit is identical to open circuit terminated microstrip. For frequencies where part of energy is transmitted and part is reflected the circuit model provides for an interpolation between the extremes considered above. For small dielectric

constants like 2.32 used here Lewin's form factors are 1.04 and 0.61 for open circuit termination and corner respectively.

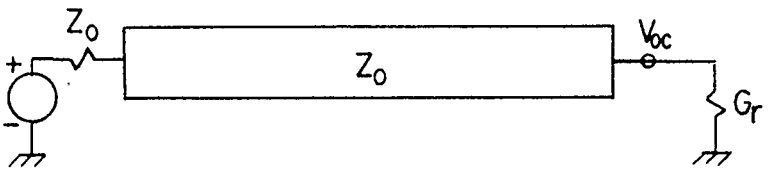

open circuit termination $P_{oc} = V_{oc}^2 G_r$

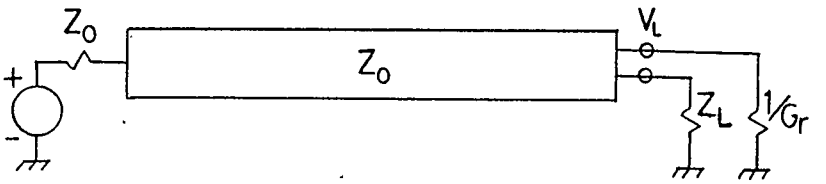

Source side leg of corner

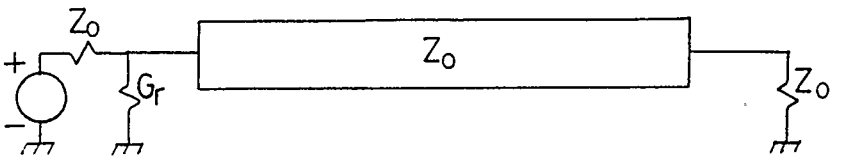

Load side leg of corner

Figure 4.6 Transmission line presentation of corner.

The transmission coefficient decreases steadily until it reaches the first null where all of the incident energy is reflected. In this frequency band the discrepancy pointed out above is largest for very low frequencies. Because radiation increases with the square of frequency any error at frequencies where the transmission coefficient is close to unity is not significant.

Comparing the power radiated as calculated by the circuit model to that predicted by Lewin (Fig. 4.12) shows that there is good agreement up to the frequency where the first null occurs. This confirms the validity of the foregoing analysis. Radiation as derived by Lewin, thus, has been successfully been reduced to a circuit level. For frequencies beyond the first null waveguide modes arise. To the best of the authors knowledge, there is no known theory that predicts radiation losses due to waveguide modes in microstrip lines. A possible method of treating radiation from these modes will be suggested in Chapter 6.

4.3.2. Radiation Resistance in Tee Shaped Discontinuities

In this section the radiation resistance model is applied to Tee equivalent circuits. Again, this analysis is based on Lewin's treatment of radiation from this type of discontinuities. Lewin distinguishes between two fundamental types of Tees: the side arm power divider in Fig. 4.7; and the symmetrically fed Tee in Fig. 4.8. The side arm power divider can be thought of as combination of corner and infinite line. The radiation resistances are placed in the equivalent circuit are placed in locations similar to those in a corner (see Fig. 4.5).

According to Lewin, the form factor for the symmetrically fed Tee is 0.349 for $\varepsilon_{eff} = 2.25$, and $\frac{2}{\varepsilon}$ for large dielectric constants. It is of interest to compare these values to the form factor of 0.330 and $\frac{2}{\varepsilon}$ for the matched circuit terminated microstrip.

The above comparison justifies modeling radiation in a Tee in like fashion to that of a matched termination microstrip (Fig. 4.8). In the example given by Lewin, the source is connected as shown in the Tee equivalent circuit of Fig. 4.8. The legs connected to the loads have twice the impedance of the incoming line providing for an impedance match. Due to the frequency dependence of microstrip characteristics the impedance can only be matched for a narrow band of frequencies. For other frequencies as well as mismatched but symmetric Tees one can treat the discontinuity as a superposition of an open circuit termination and a matched Tee.

Since the above analysis parallels that of the corner, no separate experimental verification is necessary. The analyses given here can be extended to encompass all types of discontinuities treated in this thesis.

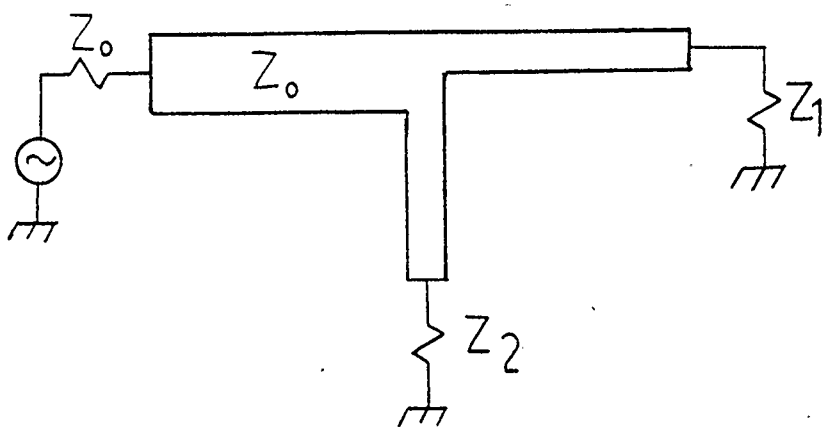

Figure 4.7 Side arm power divider.

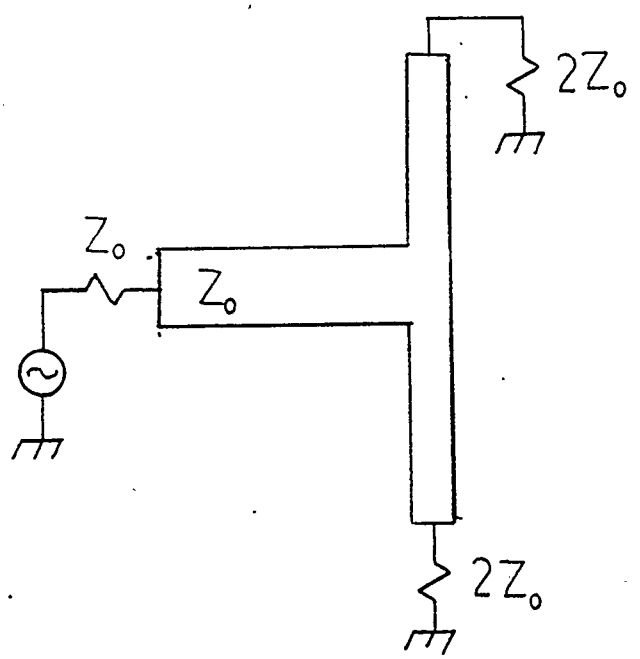

Figure 4.8 Symmetrically fed T-junction.

4.3.3. Experimental Verification

Fig. 4.9 shows the scattering parameters for a 50-50 Ω corner calculated with and without radiation resistances in the circuit. A comparison of the S_{11} and S_{21} parameters indicate that the reflected signal loses more energy to radiation than the transmitted signal. Measured results are also given in Fig. 4.9. These measured results are not only affected by radiation from the discontinuity but by resistance and dielectric losses and by radiation from microstrip - coax transitions effects as well.

To isolate losses that are not directly related to the discontinuity, scattering parameters of a straight section of microstrip line are also measured. The total length of the line used is equal to that of the corner. The results are given in Fig. 4.10. Fig. 4.11 shows again the calculated and measured S_{11} parameters of the 50 - 50 Ω corner. Only calculations made for the circuit with radiation resistances in place are shown. The measured results for the corner are normalized by the results obtained from the straight section of Fig. 4.10.

Fig. 4.11 shows that losses are higher than predicted by the circuit model used. Comparing the power dissipated in the radiation resistances to that predicted by Lewin (Fig. 4.12) indicates that radiation is adequately modeled up to the first null of the S_{21} parameter. This null coincides with the cut-off frequency of the first *TE* mode. It appears that losses not yet accounted for in the theoretical analysis may exist.

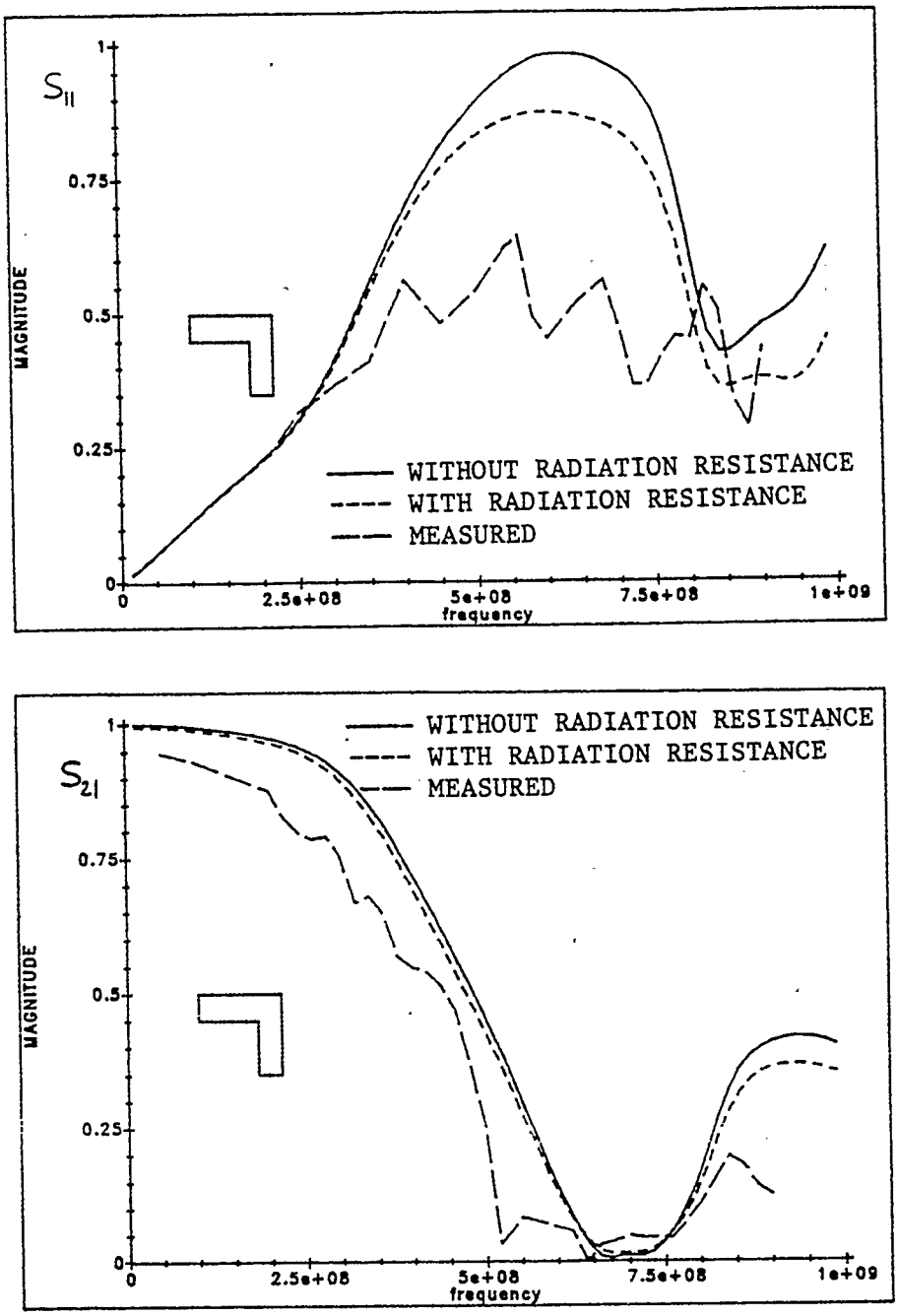

Figure 4.9 S_{11} & S_{21}, CCT-Model with and without radiation resistance and measured data.

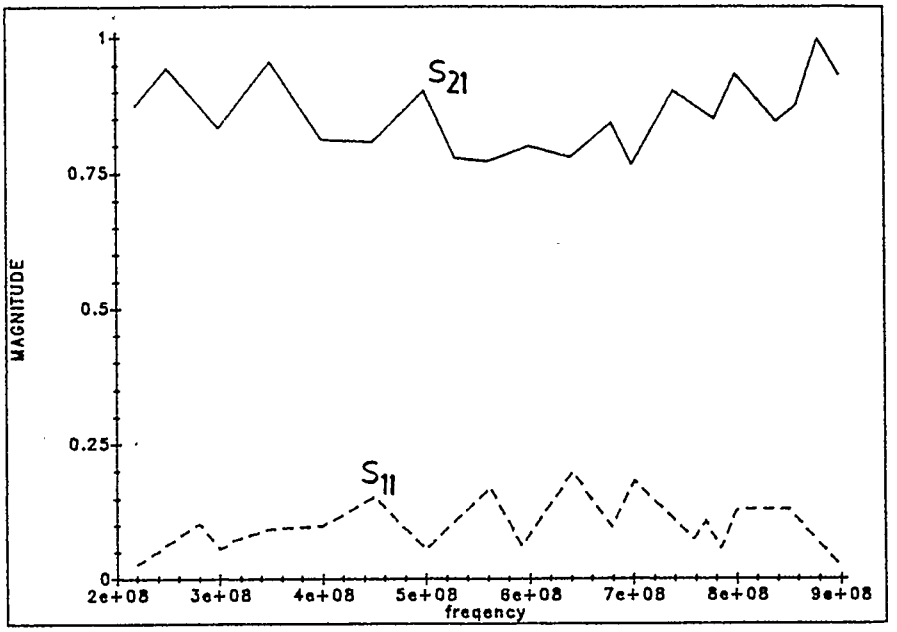

Figure 4.10 S_{11} & S_{21} for straight section of 50Ω microstrip line.

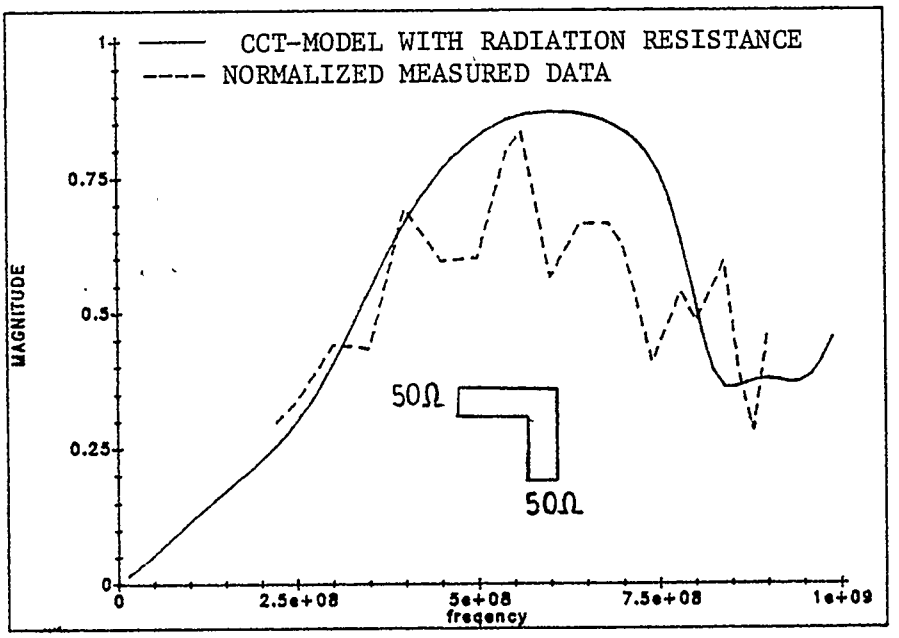

Figure 4.11 S_{11}, CCT-Model with radiation resistance and normalized measured data.

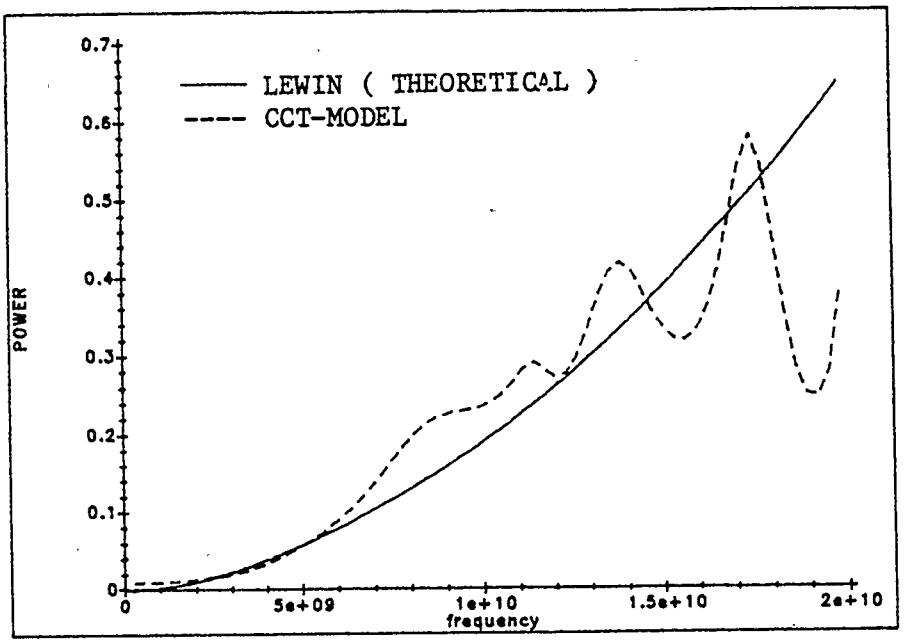

Figure 4.12 Power radiated, CCT-Model vs. Lewin's predicted radiation losses.

4.4. Surface Waves

James and Ladbrook [17] were perhaps the first to bring attention to the significance of surface waves launched from microstrip discontinuities. Their measurements indicate that for a line on an aluminia substrate, ($\varepsilon_r = 9.8$, $\varepsilon_{eff} = 6.6$, $w = 0.5cm$), that surface waves emerging from microstrip open circuits have amplitudes of 10 to 20 % that of the incident fields.

James and Ladbrook derived a transmission coefficient T giving the ratio of surface wave to incident power.

$$T = \frac{1}{4}\frac{w}{W}\left\{\left\{\frac{\varepsilon}{\varepsilon_{eff}}\right\}^{1/4} + \left\{\frac{\varepsilon_{eff}}{\varepsilon}\right\}^{1/4}\right\}^2 \tag{4.16}$$

James and Henderson derived expressions for G_s and $\frac{G_r}{G_s}$, the two expression were derived by making different assumption in each case and the results vary as much as a factor of 10. Depending on which of the three expressions for estimating surface wave losses is used, surface waves contribute from 1 to 15 % of the total losses. It follows that a useful figure for surface wave losses must be obtained through direct measurements.

In this work measurements are made on a line terminated with an open circuit. The microstrip line is constructed such that the substrate beyond the conductor termination is removable (see section 5.5). The underlying assumption is, that with the substrate beyond the conductor removed, no energy is lost to substrate

surface waves normally launched from the discontinuity. Comparing losses with and without the removable part of the substrate shows that the energy lost to substrate waves is about 1/6 of the energy radiated. This amount accounts for the discrepancy between measured and calculated results shown in Fig. 4.11. Substrate surface wave losses and their dependence on line configuration are not well understood. Further the overall effect of these modes is not significant enough to prompt any further modification on the circuit model used.

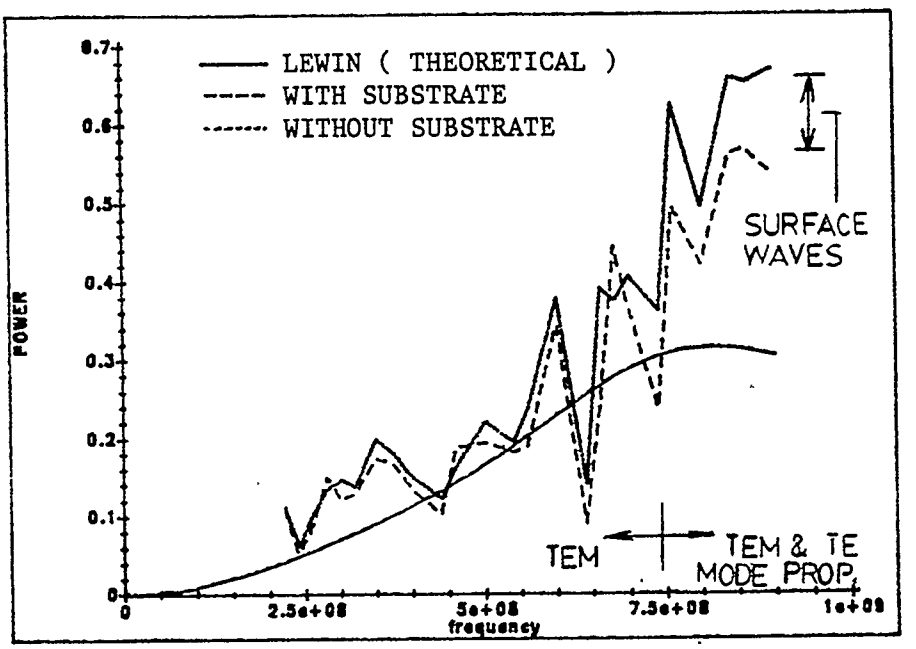

Figure 4.13 Radiation and surface wave losses.

CHAPTER 5

MEASUREMENT TECHNIQUES

5.1. Introduction

Measurement data on microstrip lines is very limited in the available literature. In addition the available data is often presented in a brief method that does not permit application to the analysis of this thesis. The focus of this thesis is on the effects of slab waveguide modes propagating in the line obtaining experimental data on these modes. Therefore, controlled experimental laboratory measurements are necessary to study these modes.

In addition, there is little or no experimental data available in the literature on radiation from various types of discontinuities. Theory predicting energy lost to substrate surface modes is inadequate for some discontinuities. In all of the above cases laboratory measurements are used to substantiate or supplement the existing theory.

Due to the nature of the project some innovative measurement techniques had to be applied. Each of these techniques and procedures along with the apparatus used are detailed in this chapter.

5.2. Apparatus

To facilitate measurement over a wide band of frequencies the microstrip circuits used were scaled in size and frequency. Scattering parameters of the fundamental mode undergo the most profound changes when waveguide modes begin to propagate. For this reason, circuit size and frequency range had to be selected such that several modes were allowed to propagate and their characteristics could be observed.

In light of these considerations, it was more convenient to take measurements in the VHF band (10-900 MHz) instead of the microwave band (1-30 GHz) where microstrip circuits are normally employed. To compensate for this reduction in frequency, the microstrip circuits were increased in size. The size and frequency range was chosen so that the first three TE modes could propagate.

Due to the large size of the microstrip conductor special care was required in designing coax-microstrip transitions. To provide for a smooth transition of the two transmission media, the substrate and the conductor were tapered to provide for a constant w/h ratio.

Figs. 5.1 and 5.2 show the circuit and the coax-microstrip transition respectively. The circuit in Figure 5.1 was used to measure the voltage distribution across the conductor.

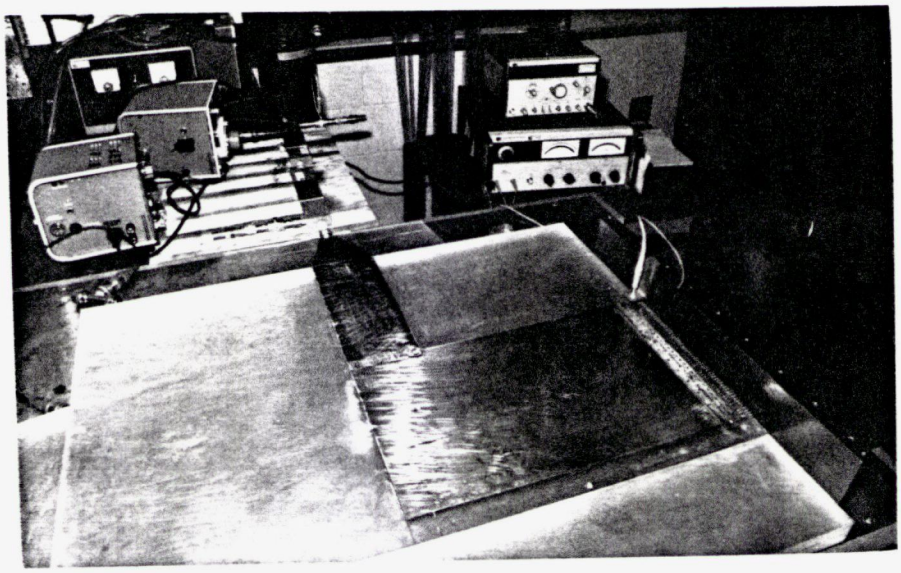

Figure 5.1 Scaled Microstrip Discontinuity

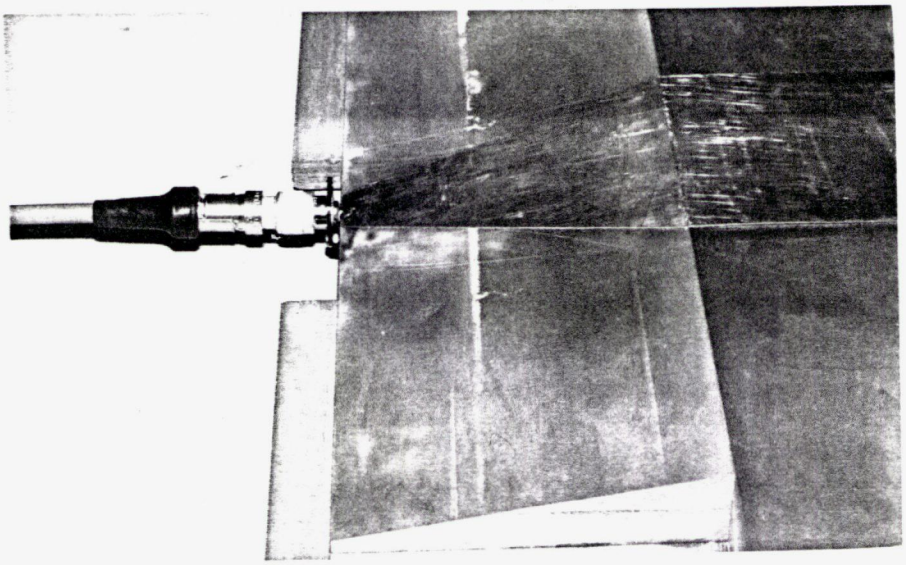

Figure 5.2 The coax to microstrip and tapered microstrip transitions are shown.

5.3. Scattering Parameter Measurements

Scattering parameters were measured with a circuit similar to that shown in Fig. 5.1. For all discontinuities used in the laboratory line impedances of 25 or 50 Ω were used. One or two parallel 50 Ω lines or terminations were used to feed or terminate the circuit under consideration. Scattering parameter measurements were made up to a maximum frequency of 520 MHz. At this frequency the fundamental and the TE_{10} mode can propagate. To provide a suitable termination for both modes, the tapered portion of the 25 Ω line conductor was split in the center (see Fig. 5.3.). The voltage distribution associated with a TE_{10} mode can only be sustained on a continuous conductor if the conductor width is larger or equal to half a wavelength. While the line impedance is held constant at the tapered microstrip-coax transition, the conductor width and therefore the cut-off frequency of the *TE* mode change. To overcome this problem the tapered part of the conductor is electrically split. The voltage change from one side of the conductor to the other can, thus, be sustained at the termination and reflection of the TE_{10} mode is virtually eliminated.

Unlike the microstrip line, the characteristics of the coaxial terminations used, change very little with frequency. The intrinsic impedance of a microstrip line changes with frequency according to equation (5.1). Terminations are therefore, only matched at low frequencies. The ripples in the measured data is a result of reflections from mismatched terminations which cannot track the changing Z_o of the microstrip line.

Results of these measurements are shown in Section 2.4. These measurements facilitate the most significant test of the 2D-circuit model. It is, of course, more important that calculated results compare well with measurement data than those calculated with different methods.

From equations (1.19), (1.20) and (1.21)

$$Z_o(f) = \frac{h\,\mu_o}{w_{eff}(f)\,\sqrt{\varepsilon_{eff}}} \tag{5.1}$$

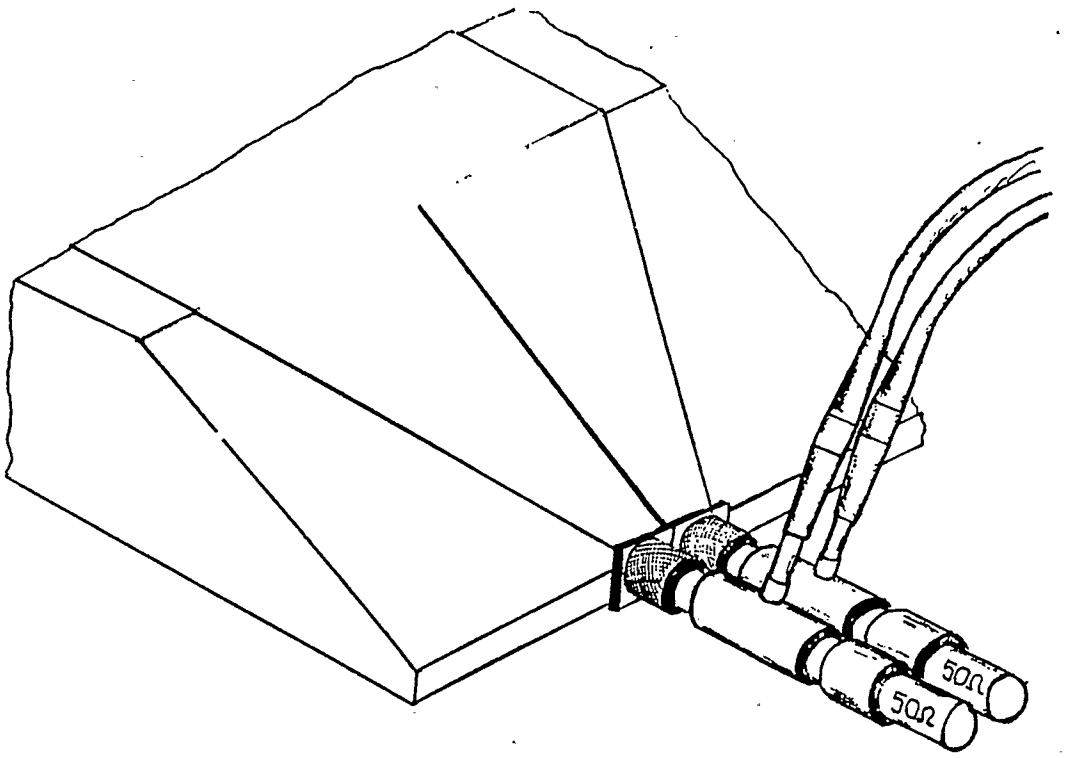

Figure 5.3 25Ω Termination.

5.4. Voltage Distribution Measurements

As shown in Chapter 2 *TE* modes result in a sinusoidal voltage distribution across the conductor. While this voltage distribution is difficult to measure at microwave frequencies on a conductor that is only a few millimeters wide, the scaled up circuit used here is very suitable for this purpose. The scaled up circuits facilitates measurements at VHF frequencies on a conductor which is large compared to the measuring probe.

Instead of the usual tapered termination, a large number of resistors were connected between conductor and a vertical extension of the ground plane. As shown in Figure 5.4 a voltage probe can conveniently and accurately be moved across the conductor. A second probe is used to to ensure a constant input and also as a phase reference.

The total parallel impedance of all resistors is equal to the intrinsic impedance of the line (25 Ω). All waveguide modes can now propagate into the termination. Voltages were measured at points that coincide with node position in the equivalent circuit. Measured and calculated data can, thus, be compared directly.

Valuable information can be drawn from these measurements. In Chapter 3 these measurements were used to substantiate the theoretical development of the 2D-circuit model. *TE* modes calculated with the circuit model were compared to measured *TE* modes and in the process radiation from *TE* modes could be estimated.

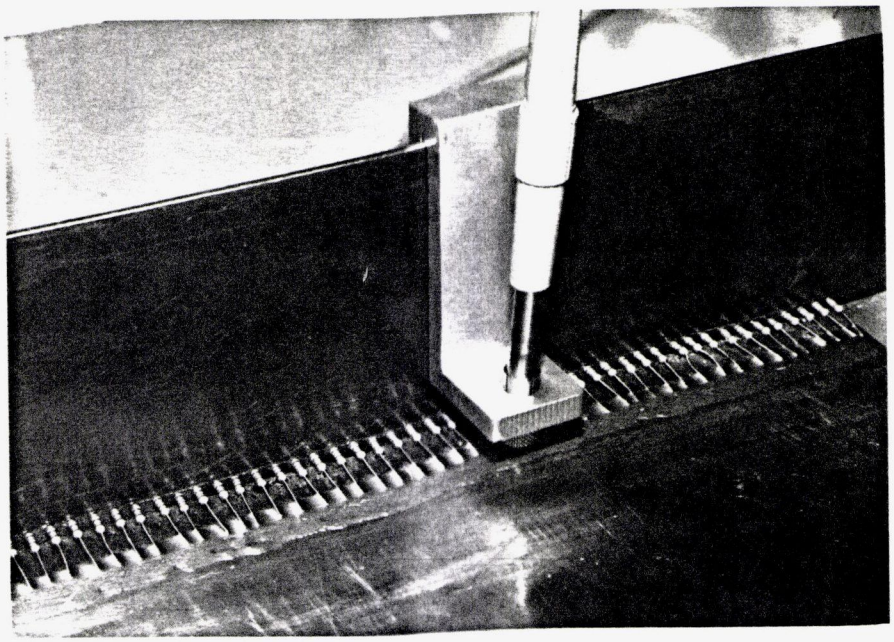

Figure 5.4 Voltage distribution measurements.

5.5. Radiation and Substrate Surface Wave Losses

Scattering parameters were measured for both circuits in Fig. 5.5. By comparing losses in both circuits radiation and substrate surface wave losses can be isolated. The radiation model of Chapter 4 was developed with the aid of Lewin's analysis. Lewin's analysis is valid only for *TEM* modes. Also, his expression for radiation losses from a corner assumes the corner consists of the perpendicular connection of two lines of equal impedance. Hence, a 50-50 Ω corner was used for these measurements.

The losses measured in the above comparison include radiation and substrate surface waves excited at the corner. To establish how much of the energy is radi-

ated and how much is launched in form of surface waves, additional measurements were taken.

James and Ladbrooke [17] suggest that substrate surface waves can be suppressed by removing part of the substrate extending beyond the conductor at the point where these modes are excited. The circuit in Figure 5.6 was used for these measurements. With the substrate in place, substrate surface waves and radiation contribute to losses. With the substrate removed, surface waves are suppressed. The difference between the reflection coefficient when the substrate is in place and when it is removed gives a quantitative indication of the amount of power that goes into the substrate waves as opposed to that radiated into free space (see Fig. 4.13).

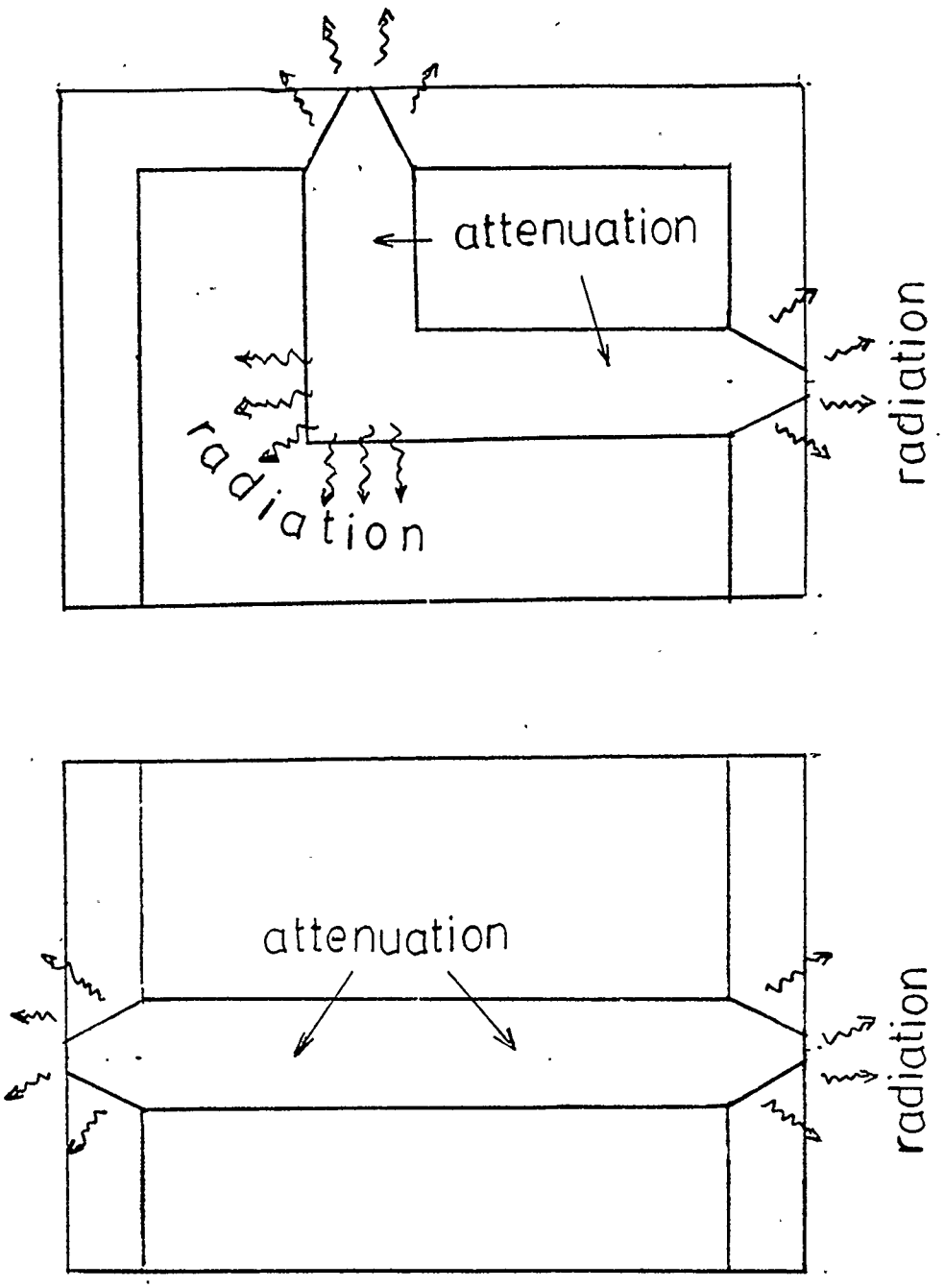

Figure 5.5 Circuits used to measure radiation and substrate surface waves

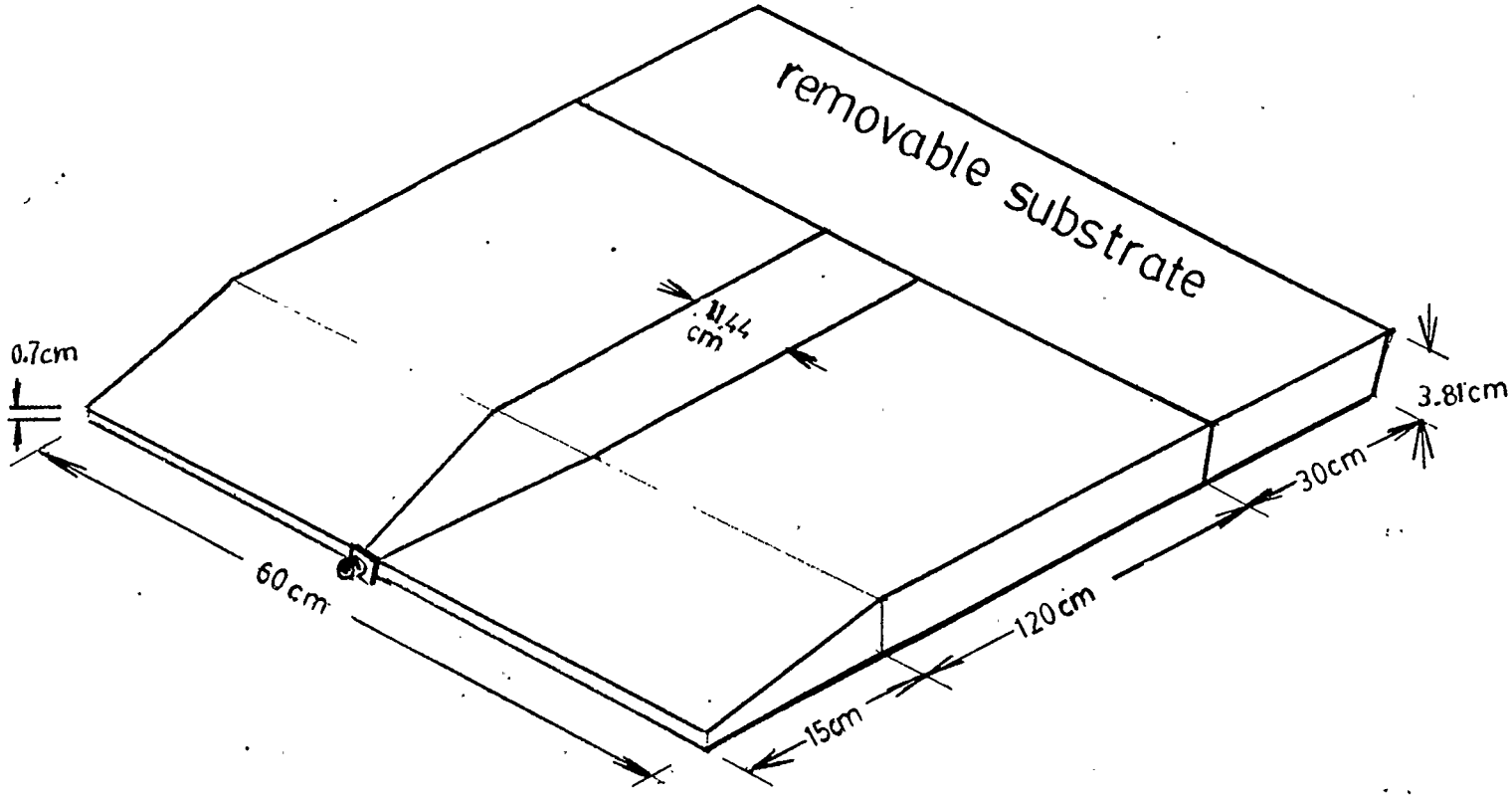

Figure 5.6 Circuit to measure substrate surface wave losses.

CHAPTER 6

CONCLUSIONS AND RECOMMENDATIONS

6.1. Conclusion

In chapter two an equivalent circuit suitable for the calculation of scattering parameters of microstrip discontinuities was developed. Numerous discontinuities were analyzed to establish the versatility and accuracy of this model.

While the accuracy of the results is quite good, the true merit of this model lies in the simplicity of its application. This equivalent circuit can be used by designers who may not be very familiar with more complex analytical tools available in microwave engineering. Boundary conditions are built into the model, hence, a background in circuit analysis is sufficient to use the model presented here.

In Chapter three it was found that slab waveguide modes have profound effects on circuit operation. At frequencies where the effective width of the conductor reaches half a wavelength a significant portion of the signals energy is coupled into waveguide modes. It has been demonstrated that these modes are largely responsible for the frequency dependence of the *TEM* scattering parameters. Perhaps more importantly, discontinuities in close proximity have a mutual affect on each other. Repeated reflections of fundamental and higher order modes result in a complex interaction between these discontinuities. This is a possible pitfall to

the designer as the prediction of scattering parameters of components by considering the interaction of the scattering parameters of individual discontinuities only for the fundamental mode will often lead to erroneous results. While many researchers consider higher order modes in their analysis of *TEM* scattering parameters, in the literature there is little or no attention given to the circuit wide effect of these modes. As shown in Figs. 2.37, 2.38, 3.6(a) and 3.6(b), groups of discontinuities in close proximity can be modeled with the method developed in this thesis. By using one equivalent circuit for two or more discontinuities the modal interaction between discontinuities described above is accounted for.

Another concern of great significance is radiation from microstrip discontinuities. Radiation increases with the square of frequency, and therefore cannot be neglected at higher frequencies. Individual scattering parameters of a given discontinuity are affected differently by radiation. For example, for a corner, the reflection coefficient loses much more energy to radiation than the transmission coefficient. This again affects the operation of the entire microstrip circuit. It is therefore imperative to consider radiation in any microstrip discontinuity analysis. Radiation conductance developed for a microstrip open circuit has successfully been modified such that it can applied to all discontinuity types considered in this thesis. The scope of the method present here has, thus, been extended beyond that of full wave analysis.

A very useful, accurate and most of all simple model has been presented. While this model can be used for a variety of discontinuities there is potential for

improvement. A rigorous understanding of higher order modes, radiation and how each relates to the circuit model needs to be explored further. In the following section a number of potential options for expanding or improving on the research presented here will be considered.

6.2. Suggestions For Further Research

Perhaps the most serious limitation of the model developed in this thesis is that it only applies to discontinuities with a Manhattan type geometries. The simplest and most obvious way of dealing with irregular shapes is by approximating the conductor shape with a large number of nodes. Once enough nodes to form more intricate shapes are used, the simplicity of the analysis would, however, be lost or offset by increased computer time. Wojciech K. Gwarek [18] uses 2D-equivalent circuits to analyze arbitrarily shaped planar circuits. While his analysis is based on the finite difference method, it seems likely that his method of dealing with irregular shapes can be adapted to the circuit formation given in this thesis.

Radiation, as treated in Chapter four, can only be modeled for *TEM* propagation. Using equations for currents and fields given in section 2.2 an expression for the lateral component of strip current can be derived. Lewin's analysis can then be repeated with an additional current component. This additional current component will result in a different polarization of the radiating field from that produced by the other current components. Additional radiation resistances may, therefore be required to model radiation from *TE* modes. Most challenging, however, is the

fact that *TE* modes substantially alter the current distribution on a microstrip line. This changing current distribution must be accounted for in the equivalent circuit in order that *TE* modes radiation can be modeled correctly.

Lastly, developing a more rigorous analysis of how the equivalent circuit applies to higher order waveguide modes, as well as studying the rate of attenuation of evanescent modes in lines emerging from discontinuities may lead to an equivalent circuit that is optimized in terms of nodes. The analysis of microstrip discontinuities will, thus, be improved in accuracy and efficiency.

REFERENCES

(1) Johnston, R.H., Graham, D.A., "The frequency dependence of microstrip junction scattering parameters", *Digest of the 27 Mid West Symposium on Circuits & Systems,* Morgantown, West Virginia, June 1984.

(2) Gupta, K.C., Ramesh, Garg and Bahl, I.J., "*Microstrip Lines and Slot Lines*", Artech House Inc. Dedham, Massachusetts, USA, 1979, Chapt.1.

(3) Silvester, P. and Benedek, P., "Microstrip discontinuity capacitances for right-angle bends, T-junctions and crossings," *IEEE Trans. Microwave Theory Tech.,* Vol. MTT-21, pp.341-346, May 1973.

(4) Thompson, A. and Gopinath, A., "Calculation of microstrip discontiuity inductance," *IEEE Trans. Microwave Theory and Tech.,* Vol. MTT-23, pp. 648-655, Aug. 1975.

(5) Gupta, K.C., Ramesh, Garg and Bahl, I.J., "*Microstrip Lines and Slot Lines*", Artech House Inc. Dedham, Massachusetts, USA, 1979, Chapt.3.

(6) Hammerstad, E.O., "Equations for microstrip circuit design," *Proc. 5th European Microwave Conference,* pp. 268-271, Hamburg, September 1975.

(7) Owens, R.P., "Predicted frequency dependence of microstrip characteristic impedance using the planar waveguide model," *Electron. Lett.,* Vol. 12, pp. 269-270, May 1976.

(8) Schneider, M.V., "Microstrip dispersion," *Proc. IEEE,* Vol. 60, pp. 144-146, 1972.

(9) Menzel, W. and Wolff, I., "A method of calculating frequency-dependent properties of microstrip discontinuities," *IEEE Trans. Microwave Theory Tech.,* Vol. MTT-25, pp. 107-112, February 1977.

(10) Mehran, R., "Die frequenzabhaengigen Uebertragungseigenschaften von Streifenleitungs- T- Verzweigungen und 90^o Winkeln," *Ph.D. Thesis, Fakultaet fuer Electrotechnik der Rheinisch - Westfaelischen Technischen Hochschule Aachen.* W. Germany, February 1974.

(11) Wolff, I., Kompa, G. and Mehran, R., "Calculation method for microstrip discontinuities and T-junctions," *Electro. Lett.,* Vol. 8, pp. 177, April 1972.

(12) Lewin, L., "Radiation from discontinuities in stripline," *Proc. IEE 107C,* 1960, pp. 163-170.

(13) Sobol, H., "Radiation conductance of open-circuit microstrip," *IEEE Trans.,* MTT-19, 1971, pp. 885-887.

(14) James, J.R. and Henderson, A., "High-frequency behavior of microstrip open circuit terminations," *IEE J. Microwave Optics & Acoustics,* 1979, Vol. 3, pp. 205-211.

(15) James, J.R. and Hall, P.S. and Wood, C., "*Microstrip antenna theory and design,*" Published by Peter Peregrinus, 1981, p. 57.

(16) Lewin, L. "Spurious radiation from microstrip," *Proc. IEE,* Vol. 125, No. 7, pp. 633-642, July 1978.

(17) James, J.R. and Ladbrooke, P.H., "Surface wave phenomena associated with open-circuit stripline terminations," *Electron. Lett.* 1973, Vol. 9, pp. 570-571.

(18) Wojciech K. Gwarek, "Analysis of an arbitrarily-shaped planar circuit - A time domain approach," *IEEE Trans. MTT-33,* October 1985, pp. 1067-1072.